TECHNICAL REPORT ARBRL-TR-02462

(Supersedes IMR No. 616)

STATIC AND DYNAMIC CONSTITUTIVE EQUATIONS TO FINITE PLASTIC STRAIN FOR ROLLED HOMOGENEOUS ARMOR

Edward J. Rapacki, Jr.

January 1983

US ARMY ARMAMENT RESEARCH AND DEVELOPMENT COMMAND
BALLISTIC RESEARCH LABORATORY
ABERDEEN PROVING GROUND, MARYLAND

Destroy this report when it is no longer needed.
Do not return it to the originator.

Secondary distribution of this report is prohibited.

Additional copies of this report may be obtained from the Defense Technical Information Center, Cameron Station, Alexandria, Virginia 22314.

The findings in this report are not to be construed as an official Department of the Army position, unless so designated by other authorized documents.

The use of trade names or manufacturers' names in this report does not constitute indorsement of any commercial product.

REPORT DOCUMENTATION PAGE

READ INSTRUCTIONS BEFORE COMPLETING FORM

1. REPORT NUMBER: Technical Report ARBRL-TR- 02462
2. GOVT ACCESSION NO.:
3. RECIPIENT'S CATALOG NUMBER:

4. TITLE (and Subtitle): Static and Dynamic Constitutive Equations to Finite Plastic Strain for Rolled Homogeneous Armor

5. TYPE OF REPORT & PERIOD COVERED: Final

6. PERFORMING ORG. REPORT NUMBER:

7. AUTHOR(s): Edward J. Rapacki, Jr.

8. CONTRACT OR GRANT NUMBER(s):

9. PERFORMING ORGANIZATION NAME AND ADDRESS
US Army Ballistic Research Laboratory
ATTN: DRDAR-BLT
Aberdeen Proving Ground, MD 21005

10. PROGRAM ELEMENT, PROJECT, TASK AREA & WORK UNIT NUMBERS:

11. CONTROLLING OFFICE NAME AND ADDRESS
US Army Armament Research & Development Command
US Army Ballistic Research Laboratory
Aberdeen Proving Ground, MD 21005

12. REPORT DATE: January 1983

13. NUMBER OF PAGES: 50

14. MONITORING AGENCY NAME & ADDRESS (if different from Controlling Office):

15. SECURITY CLASS. (of this report): Unclassified

15a. DECLASSIFICATION/DOWNGRADING SCHEDULE:

16. DISTRIBUTION STATEMENT (of this Report)

Approved for public release; distribution unlimited.

17. DISTRIBUTION STATEMENT (of the abstract entered in Block 20, if different from Report)

18. SUPPLEMENTARY NOTES

This report supersedes BRL-IMR-616 (August 1978).

19. KEY WORDS (Continue on reverse side if necessary and identify by block number)

Armor, rolled homogeneous armor, constitutive equations, dynamic elastic limit, plasticity, elasticity, stress wave propagation, strain gages, impact loading, compression tests, stress-strain diagrams, dynamic plasticity, dynamic elasticity, duration of impact, coefficient of restitution

20. ABSTRACT (Continue on reverse side if necessary and identify by block number)

Experimentally determined quasi-static and dynamic constitutive equations of the form $\sigma-\sigma_y = \beta(\varepsilon-\varepsilon_y)^{\frac{1}{2}}$ are reported for rolled homogeneous armor steel. The quasi-static compression data are characterized by a parabolic response function, the origin of which lies at the yield point. Two deformation moduli β, are required to describe the data to six percent strain, and both are predicted by a mode index and transition strain structure of a general theory of plasticity. Dynamic strain, duration of impact, and final strain distribution

are measured on specimen rods subjected to axial, symmetric, constant velocity impacts over a range of 20 to 100 meters per second. The dynamic yield stress is higher than the quasi-static, but equal to the stress at a transition strain of the quasi-static curve. Dynamic strain profiles establish the applicability of a one-dimensional, rate independent, finite amplitude wave propagation theory. The dynamic response function determined is also parabolic, with its origin at the dynamic yield point, and a single deformation modulus equal to the initial quasi-static value applies. This dynamic response function accurately predicts wave velocities and strain maxima to over four percent strain. Thus, it is shown that the form of the quasi-static plastic response function is preserved in dynamic loading, and that the increase in dynamic stress is in the elastic region.

TABLE OF CONTENTS

LIST OF ILLUSTRATIONS

I. INTRODUCTION

Military specification armor steel, herein referred to as rolled homogeneous armor (RHA), is important in ballistics not only because of its use on combat vehicles to resist penetration and blast damage, but also as a target material in the research laboratory to evaluate the performance of new penetrator designs and materials. An effective evaluation requires a knowledge of penetrator-target interactions, which include the initiation, propagation and interaction of large amplitude stress waves in both target and penetrator. A knowledge of the stresses, strains, particle velocities and displacements in the target material would aid in the understanding and modeling of the penetration process. This understanding then could be applied to designing the configuration and placement of armor on combat vehicles and fortifications.

The dynamic mechanical parameters mentioned above also should be related in a general analytical form, that is, a constitutive equation, as this form lends itself readily and with flexibility for use in situations involving combined loading. Thus far, the only analytic relationships among the mechanical properties variables for RHA are for elastic deformations,[1,2] where Hooke's law applies, and for shock loading where a Hugoniot equation is applicable.[3]

The latter was deduced from plate impact experiments, and the former by an ultrasonic resonance technique and tensile stress-strain tests performed at two different strain rates. Both strain rates ($\dot{\varepsilon}$), however, were such that wave propagation effects could be safely ignored ($\dot{\varepsilon} < 1\ s^{-1}$), and little difference in material properties was discernable between data obtained at the different rates. Although stress and strain are recorded beyond the ultimate stress at both strain rates, no attempt is made to develop an analytical model for the post-yield deformation behavior.

The objectives of this study of the deformation of RHA are:

- obtain compatible uniaxial stress quasi-static and dynamic post-yield deformation data
- examine the dynamic data as a wave propagation phenomenon, and examine both types of data in the context of extant finite deformation theory

---

[1] *R. F. Benck, "Quasi-Static Tensile Stress Strain Curves--II, Rolled Homogeneous Armor," BRL Memorandum Report No. 2703, Ballistic Research Laboratory, Aberdeen Proving Ground, Maryland, November 1976, AD #B016015L.*

[2] *R. F. Benck, J. L. Robitaille, "Tensile Stress Strain Curves--III, Rolled Homogeneous Armor at a Strain Rate of 0.42 s^{-1}," BRL Memorandum Report No. 2760, Ballistic Research Laboratory, Aberdeen Proving Ground, Maryland, June 1977.*

[3] *G. E. Hauver, "The Alpha Phase Hugoniot of Rolled Homogeneous Armor," BRL Memorandum Report No. 2651, Ballistic Research Laboratory, Aberdeen Proving Ground, Maryland, August 1976, AD #B012871L.*

- correlate data obtained over a wide strain rate range in a unified theory of post-yield deformation for the conditions of uniaxial stress.

For a comparison of quasi-static and dynamic data to be meaningful, the deformation mode (tension or compression) must be identical over the range of strain rates examined. Although tensile stress-strain data at two essentially quasi-static strain rates exists, obtaining tensile wave propagation data to large strain is especially difficult for high strength materials such as armor steel. Compression experiments thus were chosen.

Quasi-static stress-strain curves were obtained by loading resistance strain-gage instrumented samples of RHA with an Instron testing machine equipped with a data logger, which recorded both stress and strain. Dynamic loading was attained by subjecting specimen rods to axial, symmetric, free flight impact over a large range of impact velocities. The struck rod was instrumented with resistance strain gages at several positions along its length, and the gage response used to create strain-time profiles. Additional data obtained from the impact tests were duration of impact, post impact velocity of both struck and striking specimen, and residual strain profiles of both specimens.

The quasi-static data exhibited Hookian characteristics up to a well defined yield point, and post-yield deformation obeyed Bell's general theory of parabolic plasticity.[4] The parabola's origin was at the yield point, and a discrete change in deformation modulus occurred at the first transition strain, also predicted by the theory. Dynamic yield stress was determined by the duration of impact measurements, a sensitive measure of the dynamic elastic limit because duration of impact is a minimum at the yield velocity.[4,5] The dynamic yield stress was markedly higher than the quasi-static value, and equal to the stress at the first transition strain of the quasi-static stress-strain curve, suggesting a heretofore unexamined relationship between dynamic yield stress and the transition strain structure of the Bell theory.

Elastic stresses did not propagate with only the elastic bar wave velocity, but with a two-wave structure near the impact end, which degenerated to the bar velocity at distances far from the impact end. The two-wave structure corresponded to the dilatational and shear waves. Levels of constant strain beyond yield propagated with constant velocity, thus establishing the applicability of the one-dimensional wave propagation theory of von Kármán,[6] Taylor,[7]

---

[4] *J. F. Bell, "A Physical Basis for Continuum Theories of Finite Strain Plasticity: Part I," Arch. Rational Mech. Anal., 70, 1979, pp 319-338, and "..... Part II," Arch. Rational Mech. Anal., 75, 1981, pp 104-126.*

[5] *J. F. Bell, "On the Dynamic Elastic Limit," Exp. Mech., 22, No. 7, 1982, pp 270-276.*

[6] *T. von Kármán, "On the Propagation of Plastic Deformation in Solids," National Defense Research Council Report A-29, OSRD 365, U.S.A., February 1942.*

[7] *G. I. Taylor, "The Plastic Wave in a Wire Extended by an Impact Load," Civil Defense Research Committee Report R.C. 329, British Ministry of Home Security, 1942.*

Rakhmatulin,[8] and White and Griffis.[9] The plastic wave speeds, C_p obtained were given by $C_p = \sqrt{(\partial\sigma/\partial\varepsilon)/\rho}$ with $\partial\sigma/\partial\varepsilon$ the slope of the static stress-strain curve, and ρ the mass density. The one dimensional wave propagation theory also predicts an integral relationship between particle velocity $\dot{u}$ and strain ε: $\dot{u} = \int^{\varepsilon} C_p \, d\varepsilon$, where C_p is the plastic wave speed. The symmetry of the impact allows an accurate determination of maximum particle velocity, and the measured strain maxima near the impact end agree closely with prediction when the wave speed expression as given above is the integrand.

The post-yield deformation behavior of rolled homogeneous armor has been characterized by a parabolic constitutive equation applicable over a strain rate range of several orders of magnitude. The quasi-static and dynamic stress-strain curves are not identical but are related through a general theory of plasticity.

II. THEORETICAL BACKGROUND

A. Parabolic Response Function for Plastic Deformation

Data obtained from over 2,000 large deformation tests on 27 annealed metals and 16 "as received" structural metal alloys of aluminum, copper and iron exhibit plastic constitutive equations whose general form is parabolic.[4,10,11,12,13] The full details of the theory and supporting experimental evidence can be found in the literature, but, for ready reference, the most important aspects pertaining to this study of uniaxial stress loading are included here.

---

[8] *K. A. Rakhmatulin, "Propagation of a Wave of Unloading," Soviet J. Appl. Math. Mech., 9, 1945.*

[9] *M. P. White, Le van Griffis, "The Permanent Strain in a Uniform Bar Due to Longitudinal Impact," J. Appl. Mech., 14, 1947, pp A-337 - A-342.*

[10] *J. F. Bell, The Physics of Large Deformation of Crystalline Solids, Springer Tracts in Natural Philosophy, Vol. 14, Springer-Verlag, Heidelberg, Berlin, New York, 1968.*

[11] *J. F. Bell, The Experimental Foundations of Solid Mechanics, Handbuch der Physik, Vol. VIa/1, Springer-Verlag, Heidelberg, Berlin, New York, 1973.*

[12] *J. F. Bell, "Technological Perspectives from Two Decades of Fundamental Research in Dynamic Plasticity," BRL Contract Report No. 184, Ballistic Research Laboratory, Aberdeen Proving Ground, Maryland, October 1974, AD #A003175.*

[13] *J. F. Bell, "Origins in Experiment of a New General Theory of Plasticity for Structural Metal Alloys," BRL Contract Report No. 311, Ballistic Research Laboratory, Aberdeen Proving Ground, Maryland, August 1976, AD #A029845.*

Early studies by Bell on annealed aluminum show a plastic engineering stress-engineering strain relationship given by

$$\sigma_p = \beta \varepsilon_p^{1/2} \tag{1}$$

where β - parabola coefficient, GPa

ε_p - engineering strain, mm/mm

σ_p - engineering stress, GPa

and subscript p refers to plastic conditions. The parabola coefficient varies linearly with temperature and depends on the value of the material's isotropic linear elastic shear modulus at absolute zero. It is given by

$$\beta = (2/3)^{r/2} \mu(0) B_o (1-T_a/T_m) \tag{2}$$

where r - non-negative integer mode index

B_o - dimensionless universal constant, 0.0280

T_a - material temperature, degrees Kelvin

T_m - material melting temperature, degrees Kelvin

$\mu(0)$ - isotropic linear elastic shear modulus at zero degrees Kelvin, GPa

The parabolicity is obvious when the stress-strain data are viewed as σ^2 vs. ε plots, as the slopes become linear. A similar parabolic response function applies to other metals.[14]

The slope of a σ^2 vs. ε plot need not be single valued, but may have discrete values corresponding to discrete changes in the mode index r, which may either increase or decrease. The changes in slope occur at specific values of plastic strain given by

$$\varepsilon_N = (2/3)^{N/2}/\sqrt{3} \tag{3}$$

where N may have the values 18, 13, 10, 8, 6, 4, 2, and 0, in the order of increasing plastic strain. These ε_N are transition strains, and although the physics is not yet explicable, several other physical properties exhibit radical changes when materials are deformed beyond those values.[11,*]

---

[14] *J. F. Bell, "Generalized Large Deformation Behaviour for Face-Centered-Cubic Solids: Nickel, Aluminum, Gold, Silver and Lead," Phil. Mag. 11, No. 114, 1965, pp 1135-1156.*

**J. F. Bell, "The Initial Yield and Large Deformation of Mild Steel in the Context of a General, Incremental Theory of Finite Plastic Strain," (manuscript pending publication).*

Bell[10] shows an empirical temperature dependent relationship for the linear elastic shear modulus

$$\mu(T_a/T_m) = 1.03\ (1-T_a/2T_m)\ \mu(0) \tag{4}$$

which is valid over the fractional temperature range $0.06 \leq T_a/T_m \leq 300/T_m$. This observation, along with the elastic constant relation

$$\mu = E/2(1+\nu) \tag{5}$$

where E - Young's modulus, GPa

μ - shear modulus, GPa

ν - Poisson's ratio, dimensionless

was used to modify Eq. (2) in terms of E and ν:

$$\beta = (2/3)^{r/2}\ B_o\ \{[E/1.03(1+\nu)][1-(2-T_a/T_m)^{-1}]\} \tag{6}$$

The bracketed portion of Eq. (6), designated by {} thus becomes the material property constant in the parabola coefficient.

For fully annealed materials with a negligible elastic limit, the total stress and total strain may be used in Eq. (1). Materials with an appreciable elastic limit also exhibit parabolic plasticity, but the origin of the parabola must be shifted to account for the elastic region. The counterpart of Eq. (1) is thus

$$\sigma - \sigma_y = \beta(\varepsilon-\varepsilon_y)^{\frac{1}{2}} \tag{7}$$

where σ and ε refer to total nominal stress and total nominal strain respectively, and the subscript y refers to values at yield. This region of deformation where reference is made to the elastic region is termed the intermediate, or elastic-plastic region. The parabola coefficient β has the same initial mode index as the annealed material, and changes in mode index occur in the intermediate region as well. The displacement of the parabola's origin in stress-strain space, however, must be accounted for in computing the transition strains, thus

$$\varepsilon_N' = \varepsilon_N + \varepsilon_y \tag{8}$$

where ε_N' is the total strain at which a transition can occur.

B. Dynamic Yield Condition

The yield stress and strain for quasi-static loading can be determined by locating the terminus of the linear elastic region of the stress-strain curve, or in cases where no definitive yield point occurs, by the 0.2 percent strain offset method. In either case, load and deformation can be measured directly and related to stress and strain. For dynamic loading, one may use the linear elastic energy balance equation

$$1/2\ \sigma\varepsilon = 1/2\ \rho\dot{u}^2 \tag{9}$$

and the stress-strain relation for uniaxial loading

$$\sigma = \lambda\Delta + 2\mu\varepsilon \tag{10}$$

$$[\text{or}\quad \sigma = E\varepsilon\ (10')]$$

where $\dot{u}$ - particle velocity, mm/μs

λ - Lamé's constant, GPa

ρ - mass density, g/cm^3

Δ - dilatation, mm^3/mm^3

to obtain a relation between stress and particle velocity

$$\sigma = \rho C_o \dot{u} \tag{11}$$

where $C_o = \sqrt{E/\rho}$, the elastic bar wave speed, mm/μs. This relation is valid for $\dot{u} < \dot{u}_y$, that is for particle velocities below the elastic limit velocity, and hence for elastic stresses.

Bell[4,5] shows that a measure of the duration of impact for axial, free flight collisions of two identical long rod specimens is a sensitive indicator of the end of the elastic region. Sears shows that duration of impact decreases as impact velocity increases in the elastic region.[15] Bell shows the converse is true in the plastic region, and that a minimum occurs at the transition from elastic to plastic behavior.[5] The maximum particle velocity at the minimum duration of impact is $\dot{u}_y$, which can be used in Eq. (11) to calculate dynamic yield stress.

Another determination of the particle velocity at the end of the elastic region can be made by examining the coefficient of restitution versus impact velocity. The coefficient e, is defined as the absolute value of the ratio of the final relative velocity of the specimen rods to their initial relative velocity. It remains essentially constant for elastic deformations, but begins a sharp decrease when some of the impact energy is used to produce plastic deformation, that is, at yield.

C. Plastic Wave Propagation

Plastic deformation of solids by stress waves is a complex process. Strain-time measurements on long rod specimens subjected to axial, symmetric, constant velocity impact provide experimental data amenable to a one-dimensional analysis. The analysis used is the Lagrangian form of a strain-rate independent, finite amplitude wave propagation theory.[6] The development of the theory

---

[15] *J. E. Sears, "On the Longitudinal Impact of Metal Rods with Rounded Ends, Part II," Cambridge Phil. Soc., 21, 1912, pp 49-105.*

from first principles is reproduced by Kolsky,[16] so only the most important features are shown here. The salient feature is that each level of strain propagates with a velocity dependent upon the instantaneous slope of the governing stress-strain curve, which need not be specified beforehand. This feature arises from the solution of a wave equation

$$\rho \frac{\partial^2 u}{\partial t^2} = S \frac{\partial^2 u}{\partial X^2} \tag{12}$$

where t - time, μs

u - displacement, mm

S - deformation modulus, $\partial\sigma/\partial\varepsilon$, GPa

X - Lagrangian coordinate, mm.

(This notation parallels that used by Kolsky.[16])

The deformation modulus S need not be initially specified, but must be a single valued function of strain, $S(\varepsilon)$, and the stress-strain curve must be concave toward the strain abscissa. The stress wave propagation velocity for levels of constant strain is given by

$$C(\varepsilon) = \sqrt{S(\varepsilon)/\rho} \tag{13}$$

That levels of constant strain propagate with constant velocity may be experimentally determined by comparing wave speeds for levels of strain over at least two portions of a rod subjected to a constant velocity impact. This is the first requirement to determine the applicability of the theory.

The second requirement of the theory is that a relationship between particle velocity and corresponding strain exist. Integrating Eq. (12) produces

$$\dot{u} = \int^{\varepsilon} C(\varepsilon)\, d\varepsilon \tag{14}$$

which may also be checked experimentally by comparing maximum strains and maximum particle velocities. It follows that the stress is given by

$$\sigma = \rho \int^{\varepsilon} C^2(\varepsilon)\, d\varepsilon \tag{15}$$

The wave equation [Eq. (12)] may be integrated graphically, numerically, or if the wave speeds are experimentally found to be functionally related to the strains, analytically. The results are experimentally determined particle velocity-strain and dynamic stress-strain curves.

---

[16] *H. Kolsky, Stress Waves in Solids, Dover Publications, Inc., New York, 1963, pp 164-170.*

III. EXPERIMENTAL

A. Specimen Material and Preparation

Rolled homogeneous armor is a high nickel, chrome-moly steel. Chemical analysis of the material used is presented in Table 1.

TABLE 1

CHEMICAL ANALYSIS OF[3] 38 mm RHA

Element	Weight Percent
Iron	> 94.82
Nickel	3.04
Chromium	1.07
Molybdenum	0.10/0.25
Manganese	0.27
Carbon	0.26
Silicon	0.18
Copper	0.07
Aluminum	< 0.02
Vanadium	< 0.01
Sulphur	0.008
Phosphorous	0.001
	100.00

After having been cast into ingots, the steel is hot rolled and cross-rolled to various standard plate thicknesses, and heat treated, quenched and tempered in accordance with MIL SPEC MIL 12560B.[17] The specification requires that hardness be kept within certain limits depending on plate thickness. The hardness of the thirty-eight millimeter thick plate stock from which specimens were prepared was 30-31 Rockwell C,[2] although a cyclic hardness variation across the thickness of the plate has been reported.[3]

The plate stock was saw cut into bars 38 x 38 x 300 mm. The bar's longitudinal axis was in the direction of the final roll of the plate, which was determined by a macroscopic examination of the flow lines after etching with Frye's reagent.[18] The choice of axis orientation relative to the plane

---

[17] *Military Specification, Steel Armor: Plate Wrought Homogeneous; Combat Vehicle Type (1/4 to 6 inches, incl.), MIL SPEC MIL-S-12560B (ORD), 31 July 1962.*

[18] *G. L. Kehl, Principles of Metallographic Laboratory Practice, McGraw-Hill Book Co., Inc., New York, 1949, pp 205-206, Table 28.*

of the plate was arbitrary, but a single orientation of all test specimens prevented variations in the data due to preferred orientation of the grain structure induced by rolling. The bars were machined to flat-ended cylindrical rods with a surface finish of sixty-three microinch.

The quasi-static compression specimens were 9.55 mm in diameter and 28.58 mm long, providing a length to diameter ratio, (L/D) of three to one. The foil type resistance strain gages used to measure strain were high elongation, 90 degree Tee rosettes, with 1.57 mm gage length. Each specimen was instrumented with three gages, 120 degrees apart, midway along the length of the specimen. The two gage axes of the rosette were parallel and perpendicular, respectively, to the specimen axis.

The long rod impact specimens were 25.10 mm diameter and 249.75 ± 4.45 mm long, for an L/D of ten. The impact end of each rod was ground in a jig to insure its perpendicularity to the longitudinal axis of the rod and to provide a flat surface to facilitate axial alignment of the striker and struck rods prior to impact. Rods were paired for each test using the criteria that the difference in their lengths be 0.03 mm or less. The struck specimens were instrumented with foil type resistance strain gages. A pair of 3.18 mm gage length gages, 180 degrees apart, were applied 25.0, 50.0, and 75.0 mm from the impact end, with the gage axis parallel to that of the rod. A pair of parallel, circumferential scribe lines, approximately 10 mm apart, straddled each strain gage position. The pre- and post-impact line spacings were used to determine residual strains. The striker specimens also had scribe line pairs at the same positions as the struck specimens. The scribe line and gage center position measurements were made using a travelling stage microscope.

B. Experimental Procedures

The quasi-static compression tests were performed with a standard Instron testing machine at a strain rate of 3.0×10^{-5} s^{-1}. The instantaneous resistance R, of each resistance strain gage was monitored and strain calculated by

$$\varepsilon = \sqrt{R/R_o} - 1 \tag{16}$$

where R_o is the initial resistance of the unstrained strain gage. This expression for strain results when a gage factor of $(2 + \varepsilon)$ is used. The details of the apparatus and data reduction can be found elsewhere,[19] however, measured strains, both longitudinal and lateral, were accurate to ± 0.0006 percent strain.

The experimental apparatus used for the constant velocity impact tests is schematically illustrated in Figure 1. The smooth bore gas gun had been honed to an i.d. of 25.15 mm. Compressed dry nitrogen gas was the propellant, and firing actuated by a solenoid valve. The muzzle of the 1.83 m long barrel was sufficiently ported with several 10 mm diameter holes to relieve the

---

[19] *R. F. Benck, D. A. DiBerardo, R. E. Franz, "Quasi-Static Compression Tests - S7 Tool Steel," BRL Memorandum Report No. 0367, Ballistic Research Laboratory, Aberdeen Proving Ground, Maryland, October 1980.*

propellant gas pressure so that at impact the striker was in essentially free flight with constant velocity. The impact chamber, which enclosed the muzzle and struck specimen, was evacuated to less than 100 μm of mercury pressure. The vacuum eliminated an air "cushion" between the flat impact ends. The exit port of the chamber, which led to a catch tank cushioned with textile waste, was sealed with a mylar diaphragm.

The struck specimen was supported in a cantilever arrangement with four #10-32 nylon screws. The hemispherical tip screws were threaded into the specimen holder, and contacted the specimen far from the impact end. Axial alignment was achieved by mating the ground impact ends of the striker and struck specimen in the position they would occupy at impact. (Approximately one-half of the striker's length was in the muzzle). The struck specimen's angular position was adjusted with the nylon screws until no light could be observed between the specimens, indicating total areal contact of the flat impact ends. The striker was then drawn to the breech of the gas gun.

The optical system used to measure striking velocity, duration of specimen contact, and post-impact velocity of struck and striker specimens was analogous to that which Bell[20] uses. The essential components were a collimated light field, which illuminated a velocity field, and a photomultiplier tube (PMT). A small filament DC incandescent lamp, mounted at the focus of a lens comprised the light system. Light field size was controlled by opaque baffles. The velocity field, which was an integral part of the specimen holder, consisted of a narrow open slot, 6.5 x 100 mm, across which two pairs of 2.5 mm wide metal strips had been fastened with screws. The plane of the strips was approximately 8 mm below the lowest portion of the specimens. The illuminated area was painted flat black to minimize reflections which could cause erroneous signals. Light that passed through the field slot was collected by a condensing lens and impinged on the collector of the PMT. Output voltage, which depended on the amount of light reaching the collector, was monitored with an oscilloscope.

As the striker approached the struck specimen, it covered the velocity field and less light reached the PMT, causing a decrease in output voltage. The light level remained constant as an opaque strip was traversed, as did output voltage. This constant output was easily detected as a "flat" on the oscillogram, typified by Figure 2. The time to traverse the known distance between the strips was measured with the aid of the 50 μs timing signal, and striking velocity was determined. When the specimens collided, the velocity field was completely covered and no light reached the PMT. The "dark" condition remained as long as the specimens were in contact. As the specimens rebounded and separated, the struck specimen passed over a second pair of opaque strips. This action produced the rising signal portion of the Type I trace, and the post-impact velocity of the struck specimen was determined. The striker specimen too, passed over the second pair of strips a short time later, as can be seen on the upper trace of Type II, where the recording time was ten times that of the Type I signal. The lower trace in Type II is that portion of the PMT signal during specimen contact, recorded on a faster time-base to improve resolution. Thus, time measurements on the PMT signal provided

---

[20] *J. F. Bell, "An Experimental Study of the Unloading Phenomenon in Constant Velocity Impact," J. Mech. Phys. Sol., 9, 1961, pp 1-15.*

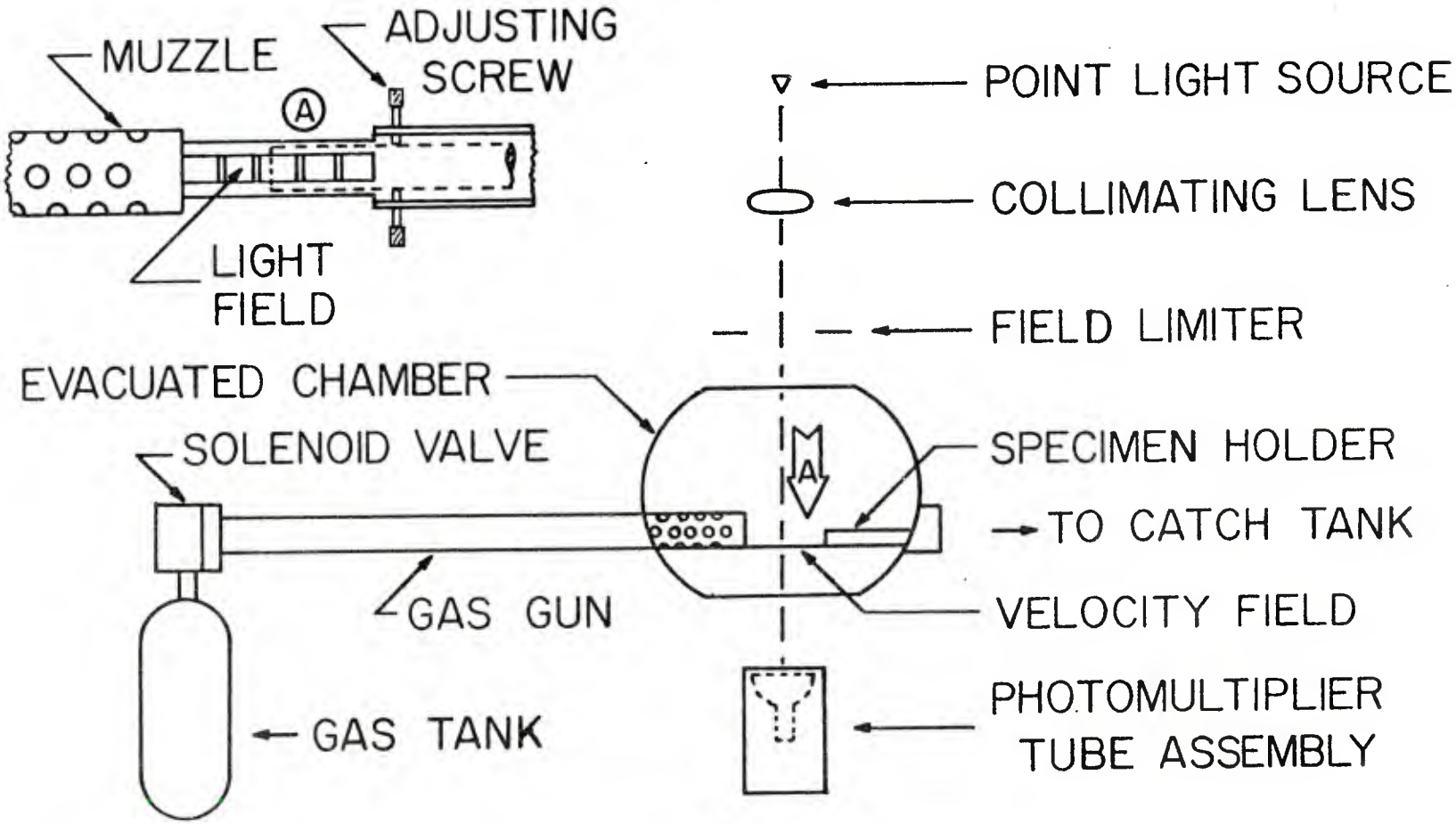

Figure 1. Schematic diagram of impact test apparatus; the optical velocity measuring field is shown in the inset.

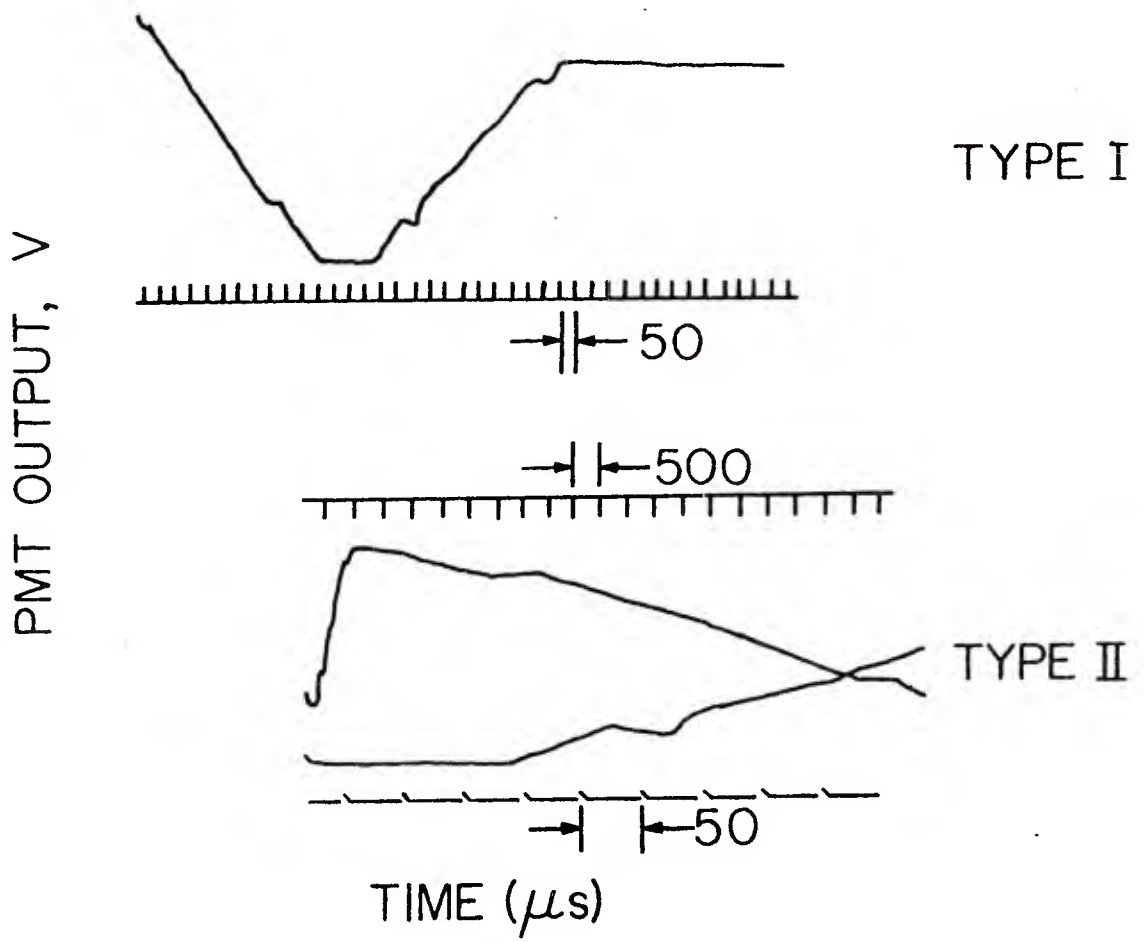

Figure 2. Typical PMT signals. Type I was recorded on time base I. Type II was delayed and recorded on time bases ten times longer (upper), and one-tenth as long (lower), as time base I.

all information needed to compute duration of impact and coefficient of restitution.

Time resolution was limited by the resolution of the digitizer used for distance measurements on the oscillograms, and the relatively long times for specimens to traverse the velocity field. Time resolution on the PMT oscillograms was typically ± 4.1 microseconds, and was the limiting factor in determining velocity, duration of impact, and coefficient of restitution. Striking velocities were accurate to within ± 0.68 meters per second. Duration of impact and coefficient of restitution values were accurate to within ± 3.2 percent and ± 2.4 percent respectively, of their determined values.

Dynamic strain measurements were made with foil type resistance strain gages, positioned as described above. Each gage was powered by an individual capacitive discharge power supply through a bridge resistance network. The current was pulsed on several microseconds before impact and shunted away from the strain gage after the recording time interval, typically 100 microseconds. Output voltage was monitored on an oscilloscope and recorded on photographic film. Calibration of strain gages and recording devices was performed before each test by introducing resistances in parallel with the strain gage and pulsing the power supply. The calibration resistances used simulated compressive strains of approximately one and five percent. The output voltages obtained during calibration were used to calculate a voltage deflection factor. The instantaneous resistance of the strain gage was determined by solution of the applicable bridge network equations, and strain was computed by Eq. (16). Dynamic strain measurements were estimated to be accurate to within ± 0.05 percent strain.

Wave speeds for levels of constant strain were determined from the characteristics of a Lagrangian diagram constructed by plotting arrival time of a level of strain versus distance from the impact end. An external estimate of the uncertainty associated with the wave speed determinations was made. The uncertainty was approximately ± 0.12 mm/μs. Wave speeds found to be constant within this limit were assumed to be constant throughout, and the characteristic was determined by least squares methods.

Residual strain at positions along the specimen rods was determined by two methods. Method one utilized the pre- and post-impact spacing of the circumferential scribe lines described above. The residual strain so determined, although distributed over a finite gage length, was associated with a rod position midway between the two scribe lines used to determine it. Method two used the pre- and post-impact diameters, which were measured with a blade micrometer, to determine diametral strain. Diametral strain was converted to longitudinal strain by assuming isochoric deformation. The residual strains determined by both methods, for both the striker and struck specimens were averaged for each position. These values were estimated to be accurate to within ± 0.024 percent strain.

IV. RESULTS

A. Quasi-Static Compression Tests

The stress-strain curves for the two quasi-static compression tests are presented in Figure 3. The initial portion of the loading curve was linear with the proportional limit at 0.812 GPa stress and 0.391 percent strain. Young's modulus is 208.0 GPa, Poisson's ratio 0.290, and the shear modulus is computed to be 80.6 GPa.

A general power function equation

$$\sigma - \sigma_y = H(\varepsilon - \varepsilon_y)^a \tag{17}$$

was assumed for the post-yield stress-strain data in nominal form, where H is the power function coefficient and a is a dimensionless exponent. A plot of the data as the common logarithm of each side of Eq. (17), where 0.821 GPa and 0.404 percent strain were used as the yield stress and strain (Figure 4), was linear with the slope (a) equal to 0.517, indicating a nearly parabolic function.

B. Dynamic Yield Stress

Fifteen symmetric, free flight, axial impact experiments were performed, with striking velocities ranging from 20 m/s to over 100 m/s. Time of specimen contact during impact and coefficient of restitution were determined. Figure 5 shows the measured time of contact (divided by specimen length to normalize variations in rod lengths) versus maximum particle velocity, which is one-half the striking velocity. The minimum duration of impact occurs at a particle velocity of 0.0236 ± .0003 mm/μs. The coefficient of restitution e, versus maximum particle velocity is plotted in Figure 6. It is essentially constant (0.932 ± .011) up to the particle velocity associated with the duration of impact minimum, after which it decreases non-linearly with increasing velocity. No permanent deformation was detected on specimen rods struck below 47.2 m/s ($\dot{u}$ = 0.0236 mm/μs).

Utilizing this value for $\dot{u}$, along with the quasi-static value of Young's modulus and a density** of 7.848 g/cm^3 in Eq. (11), the dynamic yield stress is computed to be 0.954 ± .014 GPa. The dynamic yield strain, computed with Eq. (10′), is 0.458 ± .008 percent. This value may be compared with the magnitude of the elastic precursor obtained from the resistance strain gage measurements. Figure 7 shows strain-time profiles obtained at positions 50 mm and 75 mm from the impact end of the rod, at three impact velocities. In Table 2 are the maximum particle velocities and average plastic strain rates for the data shown in Figure 7.

**Private communication from R. F. Benck, Ballistic Research Laboratory.*

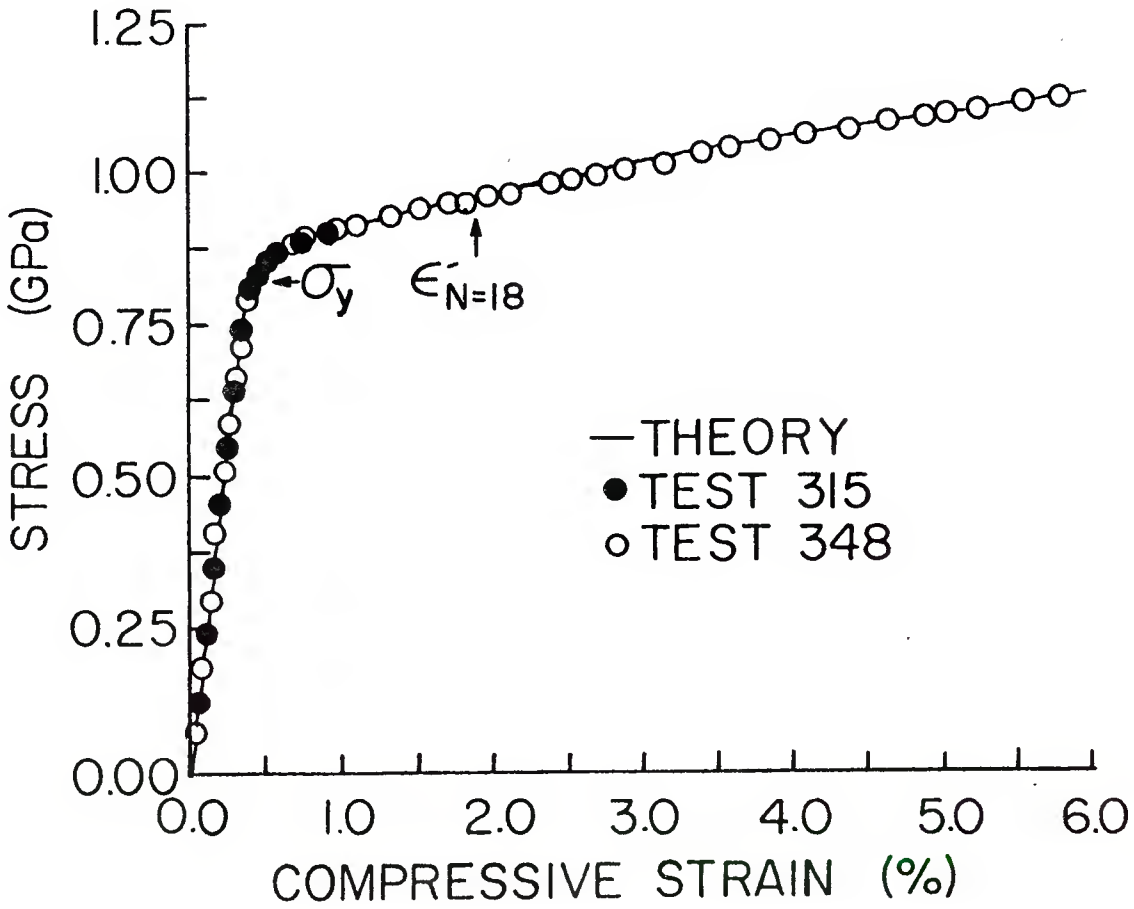

Figure 3. Stress vs. compressive strain at a strain rate of 3.0×10^{-5} s^{-1} compared with parabolic response function.

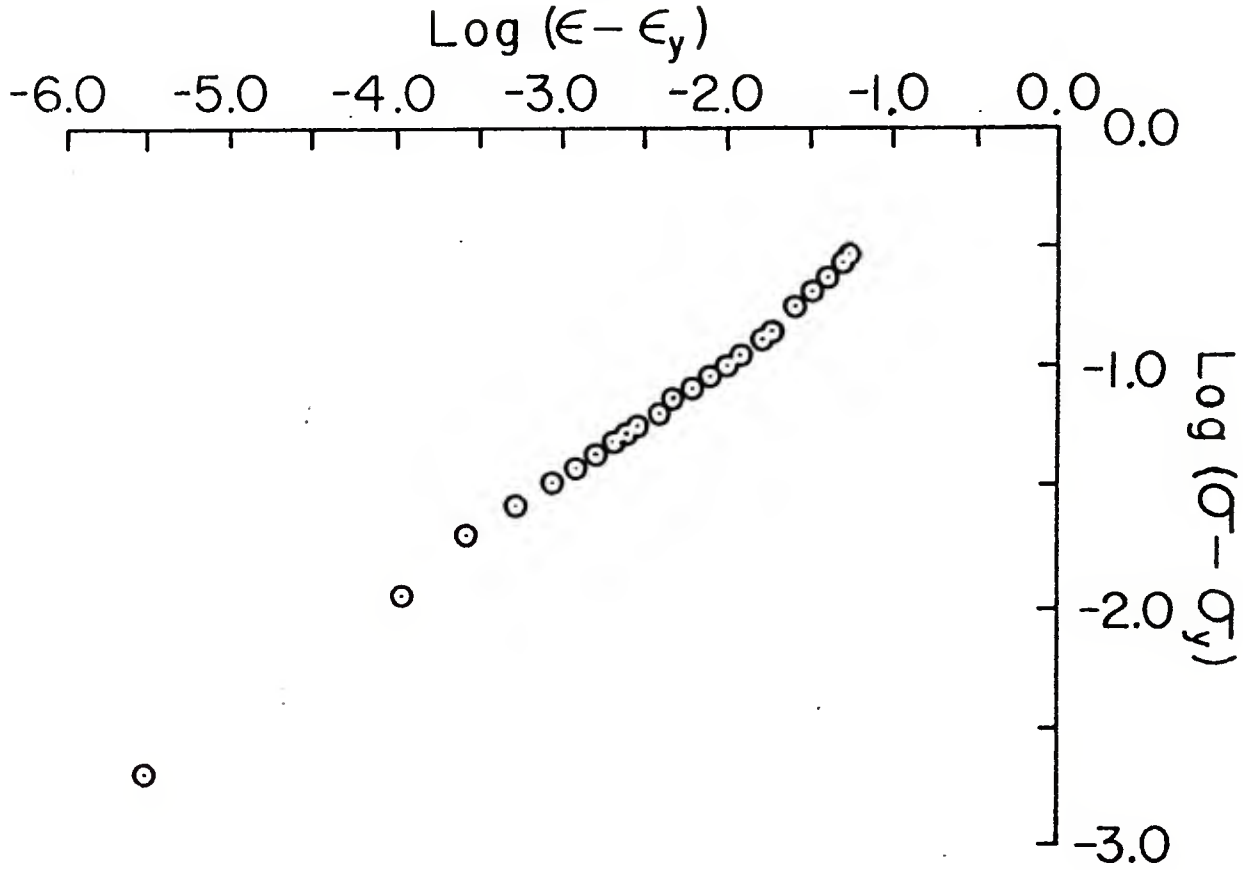

Figure 4. Log post-yield stress vs. log post-yield strain for quasi-static data. Yield stress taken as 0.821 GPa, and yield strain 0.0040.

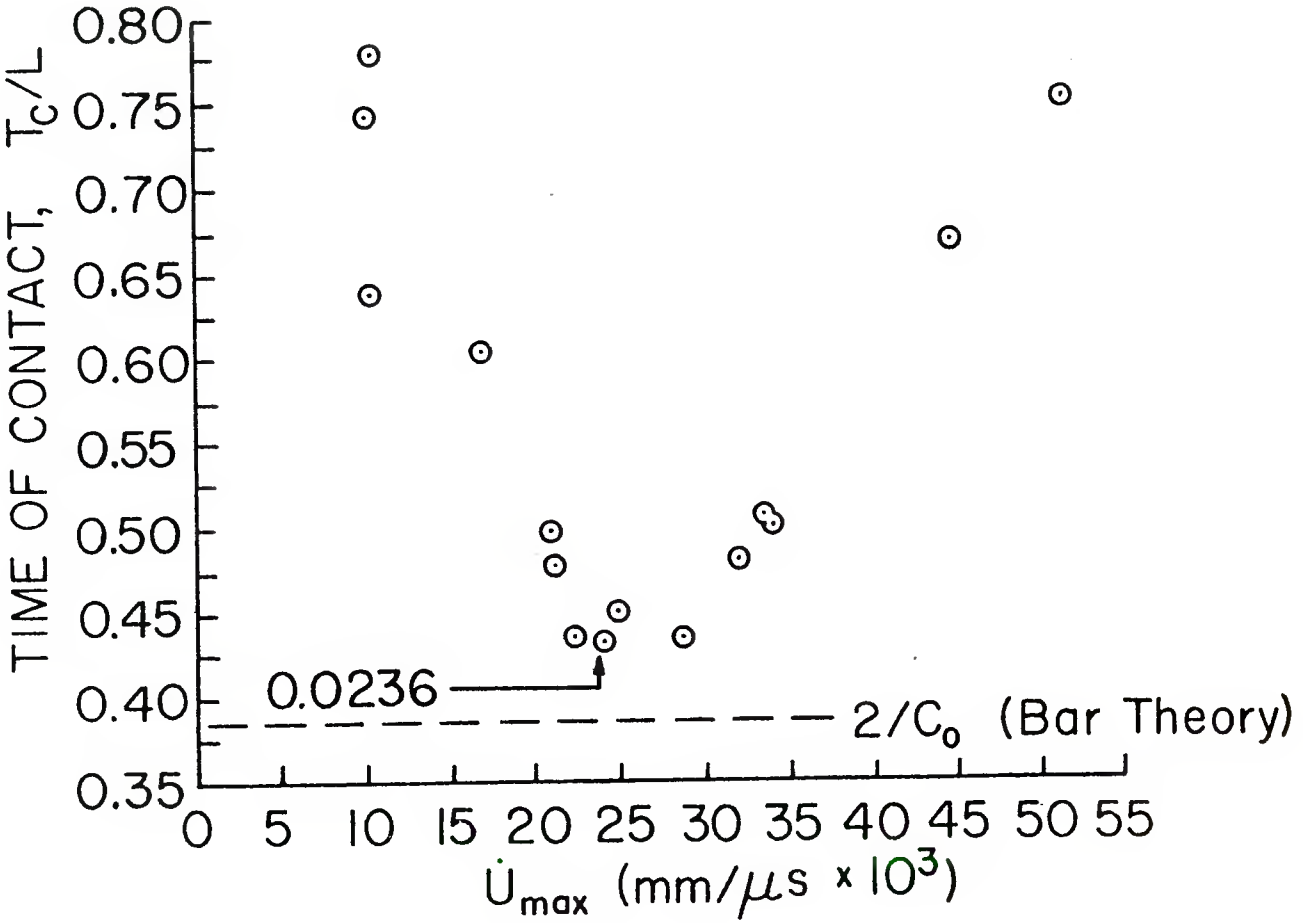

Figure 5. Normalized time of contact vs. maximum particle velocity.

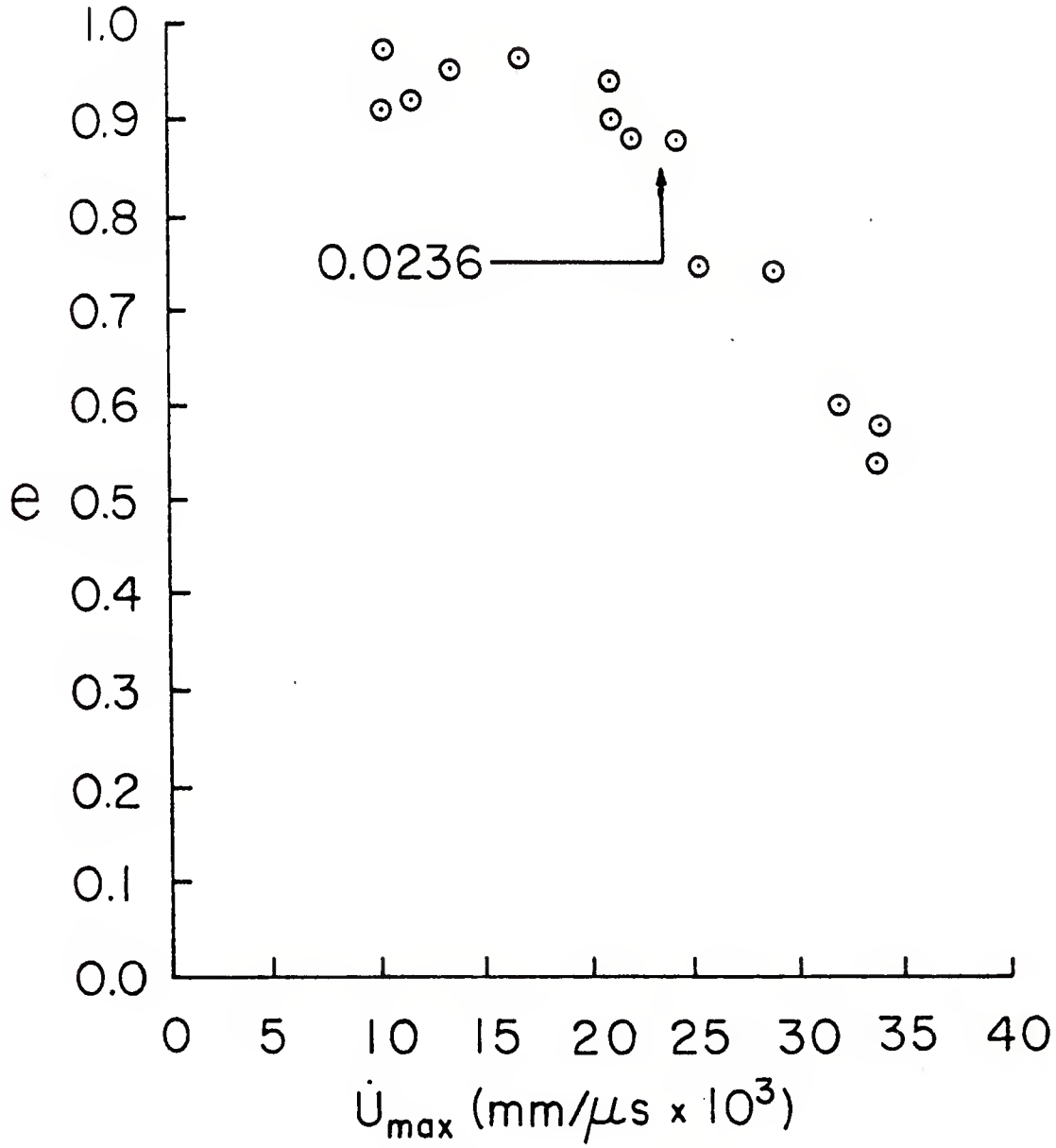

Figure 6. Coefficient of restitution vs. maximum particle velocity.

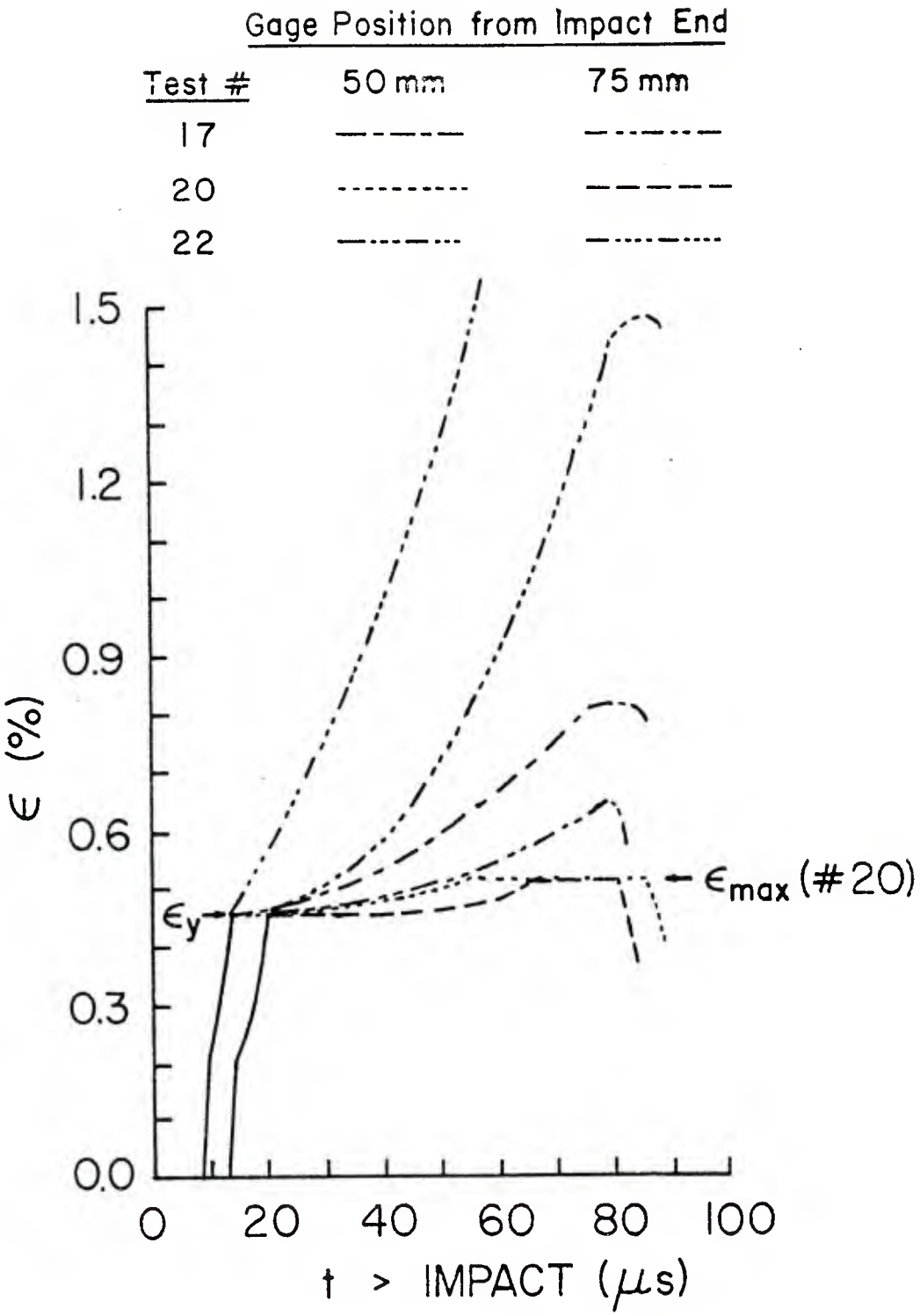

Figure 7. Compressive strain vs. time after impact at two positions on struck rod for three impact velocities.

TABLE 2

MAXIMUM PARTICLE VELOCITY AND AVERAGE STRAIN RATE

Test #	$\dot{u}_{max}$ (mm/μs)	$\dot{\varepsilon}_p$ (s^{-1})
17	0.0319	65.4
20	0.0249	14.4
22	0.0515	235.3

Although the plastic strain-rate range is larger than an order of magnitude, the computed value of yield strain is in excellent agreement with the magnitude of the elastic precursor, regardless of strain rate.

C. Elastic Wave Propagation

Examination of the elastic precursor portion of the strain time profiles of Figure 7 showed that the rise to yield strain was not linear. Wave speeds of pre-yield strains were determined, and two features were evident: (1) a two-wave structure was present, and (2) elastic strains did not propagate with constant velocity along the rod. Figure 8 shows wave speeds measured in two regions of the rod: 25-50 mm and 50-75 mm from the impact end. Also indicated are the dilatational wave velocity, C_1 given by $\sqrt{(\lambda+2\mu)/\rho}$, the shear wave velocity, C_2 given by $\sqrt{\mu/\rho}$, and the elastic bar wave velocity C_o. The first value is the average obtained from plate impact experiments,[3] 5.83 mm/μs, and the latter two computed using the quasi-static values of μ and E, and are 3.21 mm/μs and 5.15 mm/μs, respectively. In the region of the rod nearer the impact end, strains below approximately 0.20 percent strain propagated with the dilatational velocity. Strains above this value, up to the dynamic yield strain, propagated with approximately the shear wave velocity. The data of the farther region of the rod displayed a similar, although less distinct two-wave structure. The change in wave speeds occurred at the same value of strain as in the region nearer the impact end, but the wave speeds were more distributed. The statistical mode wave speeds for the strain regions above and below 0.20 percent are $\bar{C}_1$ = 5.58 mm/μs and $\bar{C}_2$ = 3.95 mm/μs.

Lamé's constant λ can be determined from knowledge of the dilatational wave speed and is computed to be 105.5 GPa. It follows that the bulk modulus K, is 159.3 GPa, and the bulk velocity of 4.51 mm/μs is in agreement with previously reported values.[3]

D. Plastic Wave Propagation

Levels of strain greater than the dynamic yield strain propagated with constant velocity beyond the first diameter length from the impact end. Increasing levels of strain propagated with slower velocities. The constancy of propagation velocity could not be determined for levels of strain which did not travel to all three strain-gage positions, so plastic wave speed data were limited to strain levels of approximately 1.4 percent strain. Single wave speeds for levels of constant strain, and decreasing wave speeds for increasing

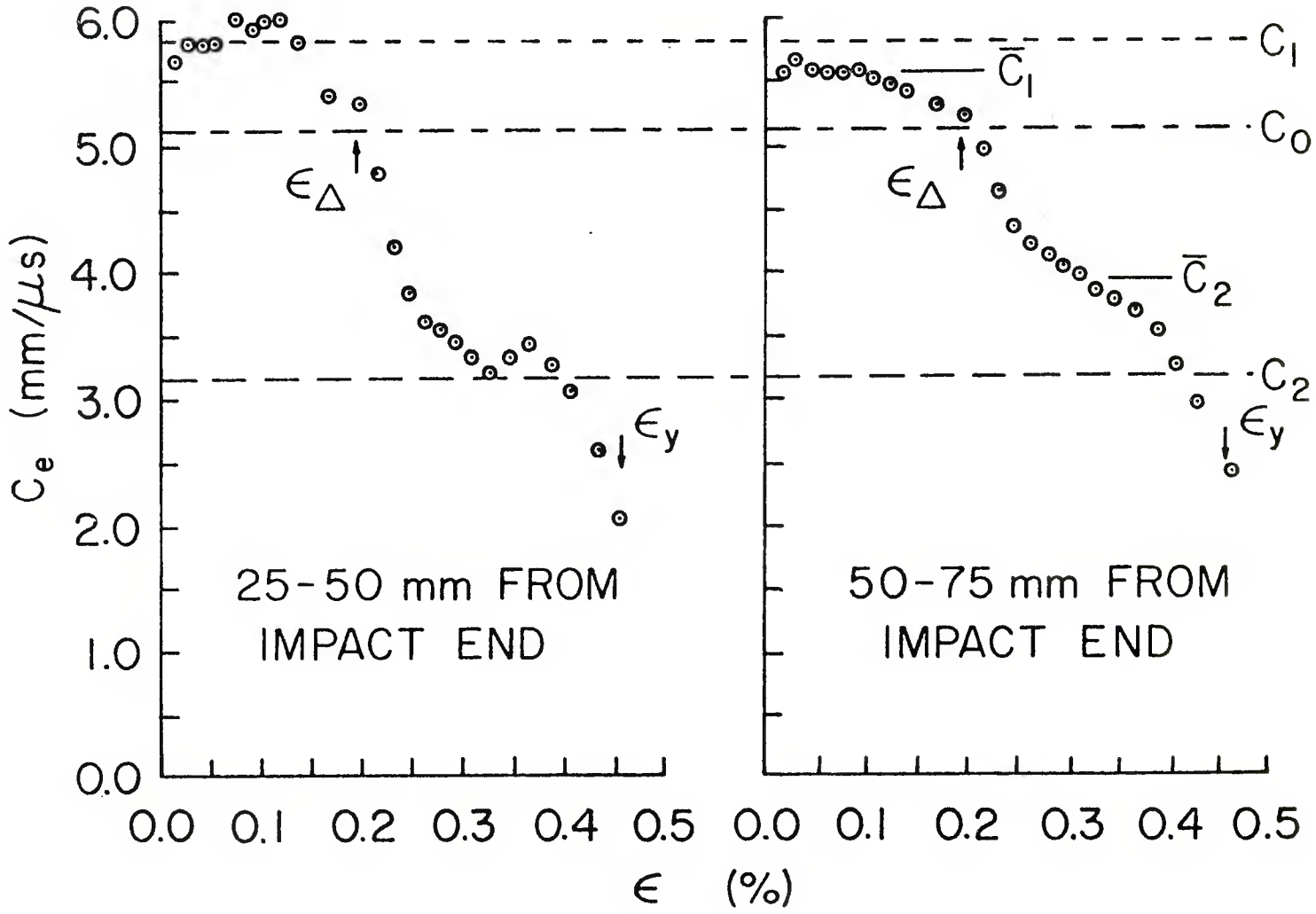

Figure 8. Wave speed vs. compressive elastic strain for two regions of the struck rod.

strains indicated that the first applicability requirement of the strain-rate independent, one dimensional, finite amplitude wave propagation theory had been met.

A general power function equation [Eq. (17)] was assumed as the governing stress-strain relationship, and differentiated to obtain an expression for wave speeds:

$$C_p = \sqrt{aH\ (\varepsilon - \varepsilon_y)^{a-1}/\rho} \qquad (18)$$

where ε_y is the dynamic yield strain. The numerator under the square root sign corresponds to the deformation modulus $S(\varepsilon)$, in Eqs. (12) and (13). A logarithmic plot of experimentally determined wave speeds versus post-yield strain is shown in Figure 9. The relationship is linear with the exponent $a = 0.522$, indicating a nearly parabolic stress-strain relationship, as was found for the quasi-static post-yield deformation.

V. DISCUSSION OF RESULTS

The experimental evidence indicating a nearly parabolic stress-strain relation suggests examination of the data in the context of Bell's[4] general theory of parabolic plasticity. The material has an appreciable elastic limit, therefore the elastic-plastic equation [Eq. (7)], if any, should apply. The parabolic response function was postulated and made linear with respect to strain. Quasi-static yield stress was determined by using the value that provided maximum piece-wise linearity (as determined by least squares methods) of the data in the post-yield stress squared-strain plane. This value was 0.822 GPa, and was very near the proportional limit stress. Figure 10 shows the data intersect the strain axis at 0.395 percent, (ε_y) also in close agreement with the proportional limit value.

An important feature is that the data are characterized by multiple slopes. According to the Bell theory, a slope change can occur at transition strains, the first of which, from Eqs. (3) and (8) with N = 18, is 1.897 percent. The intersection of the two linear segments occurs at 2.128 percent strain. This differs from prediction, however, scatter in the values of transition strains for mild steel is documented,* an exception which may also apply to steel alloys. Note, however, that no change in slope occurs at the second transition strain, $\varepsilon'_{N = 13}$.

The values of β, the deformation moduli, determined from the least squares fit slopes were found to be 1.071 GPa for $\varepsilon_y < \varepsilon < \varepsilon'_{N = 18}$ and 1.366 GPa for $\varepsilon > \varepsilon'_{N = 18}$. These may be compared with the values predicted by Eq. (6) for r = 3 (1.0868 GPa) and r = 2 (1.3311 GPa) mode indices. The calculation used the experimentally determined values of E and ν and assumed the melting temperature of iron, 1808 degrees Kelvin.[21] The experimentally determined values

---

[21] *R. C. Weast, Ph.D, ed., Handbook of Chemistry and Physics, 56th Ed., The Chemical Rubber Co., Cleveland, 1975, p B-20.*

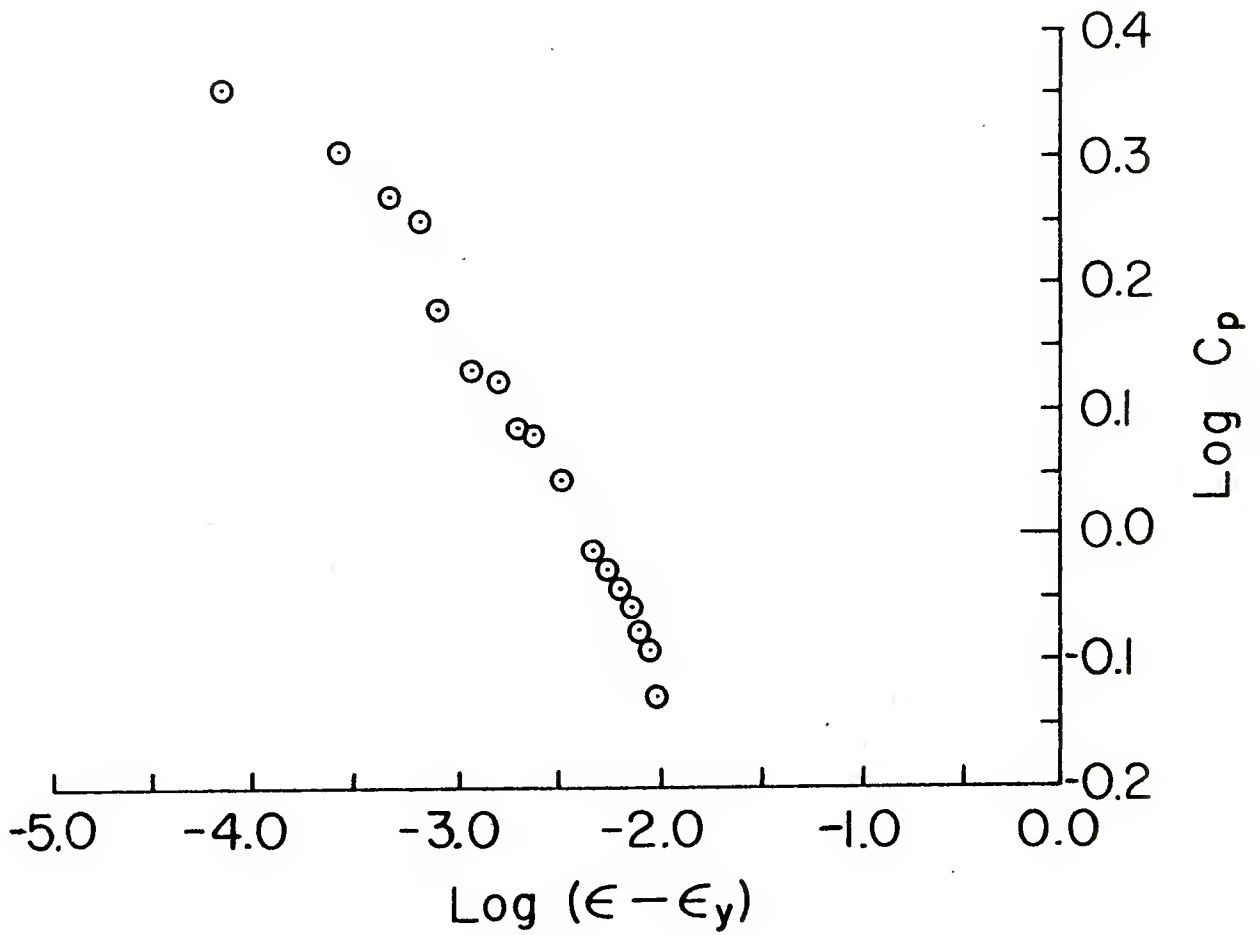

Figure 9. Log wave speed vs. log dynamic post-yield strain with yield strain 0.0046.

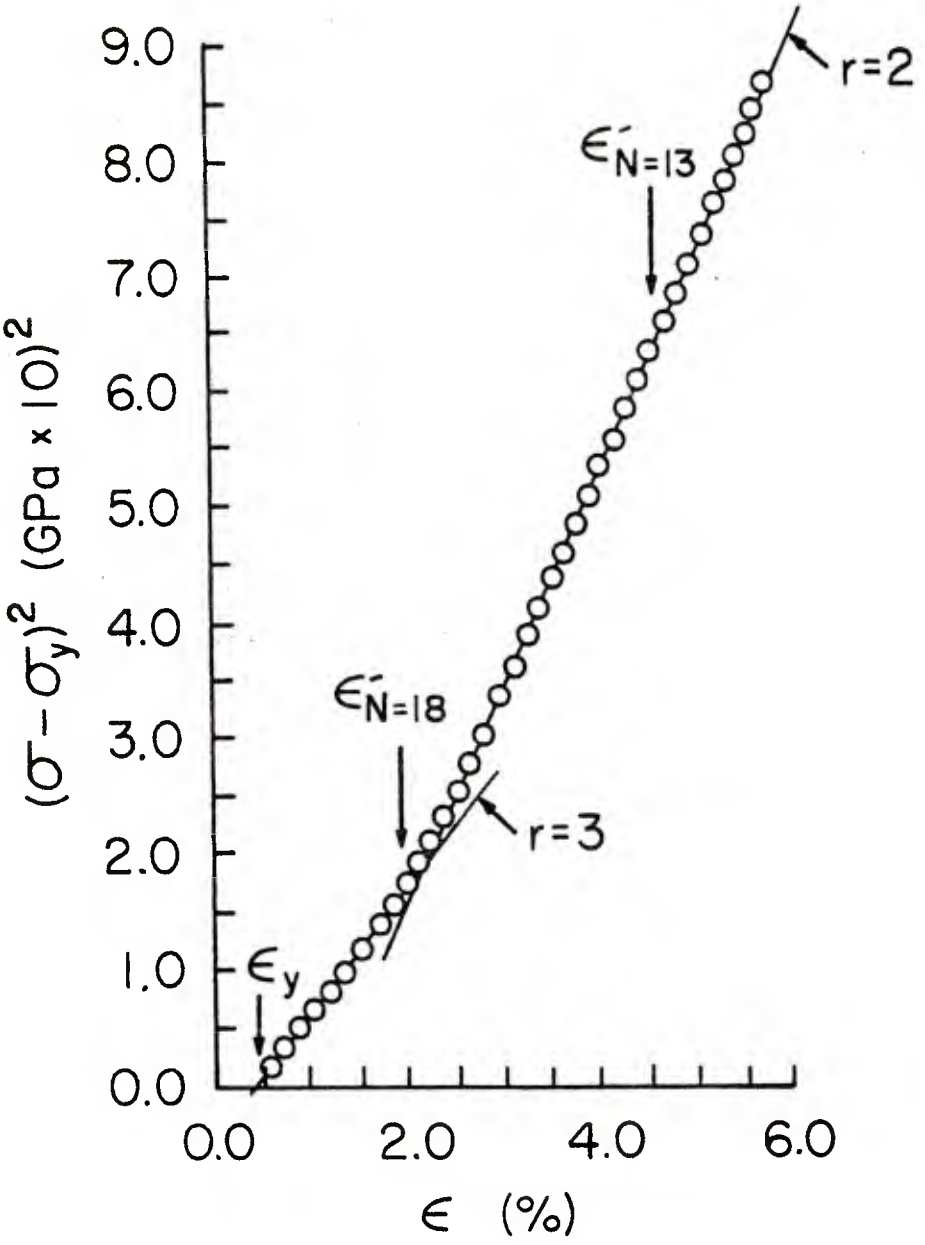

Figure 10. Post-yield stress squared vs. strain for quasi-static data; yield stress 0.822 GPa.

differ by less than two percent from the theoretical values. The correlation of theory and experiment for the entire strain range investigated is shown in Figure 3, where the parabola coefficients used are the experimentally determined values. Table 3 summarizes the constitutive equations for quasi-static loading.

The elementary bar theory of St. Venant[22] predicts that duration of impact should be independent of particle velocity and dependent only upon the length of the bar and the elastic bar wave velocity. The St. Venant theory is compared with the experimental time of contact data in Figure 5. The author believes the minimum time of contact and the bar theory should coincide, and the discrepancy is due, in part, to experimental technique. In a comparison of techniques used to measure time of specimen contact during impact, Filbey[23] shows that the optical technique used here gives values approximately seven percent longer than those obtained by electrical contact of the specimens or piezocrystal stress measurements at the impact face. Applying this correction to all the data points brings the minimum time of contact in fair agreement with the bar theory prediction. This discrepancy however, has no effect on the particle velocity value at the minimum time of contact. The curves in Figures 5 and 6 are probable curves through the data points only, and no attempt to explain their particular forms has been made.

The dynamic yield stress, found to be 16 percent higher than the quasi-static value, can be related to the quasi-static stress-strain curve by the following explanation. The stress associated with the first transition strain of the quasi-static stress-strain curve is 0.954 GPa, which is also the experimentally determined dynamic yield stress. The physical significance of this phenomenon is that a material accommodation occurs at this level of stress for both quasi-static and dynamic loading. It is interesting that the quasi-static deformation modulus increases at this stress while the dynamic modulus decreases, that is, yield occurs.

Elementary elastic wave propagation theory predicts that elastic strains propagate with the elastic bar wave velocity C_o. Studies of the initial development of an elastic pulse in a semi-infinite aluminum bar[24] show that the theory applies at large distances from the impact end, but that near the impact end, the arrival time of low level elastic strains is predicted by the dilatational velocity. The experimental data of Figure 8 show this to be true with RHA also. The maximum axial strain which may propagate with the dilatational velocity can be determined by calculating the dilatation itself. Before the passage of the shear wave, the impacted rod experiences only a wave of dilatation and is therefore in a state of uniaxial strain. The dilatation is due only to this uniaxial strain until the shear wave arrives and produces

---

[22] *S. Timoshenko and S. N. Goodier, Theory of Elasticity, McGraw-Hill Book Co., Inc., New York, 1951, p 444.*

[23] *G. L. Filbey, "Intense Plastic Waves," Ph.D. Dissertation, The Johns Hopkins University, Baltimore, Maryland, 1961.*

[24] *J. F. Bell, "The Initial Development of an Elastic Pulse Propagating in a Semi-Infinite Bar," BRL Technical Report No. 6, The Johns Hopkins University, Baltimore, Maryland, November 1960.*

TABLE 3

QUASI-STATIC CONSTITUTIVE EQUATIONS FOR 38 mm RHA IN UNIAXIAL COMPRESSION

Deformation Region	Constitutive Equation	Applicability Range, Strain	Deformation Modulus, GPa
Elastic	$\sigma = E\varepsilon$	$0 < \varepsilon < .00395$	208.0
Plastic I[a]	$\sigma = \sigma_y + \beta(\varepsilon - .00395)^{1/2}$	$.00395 < \varepsilon < .02128$	1.071
Plastic II[a]	$\sigma = \sigma_y + \beta(\varepsilon - .01064)^{1/2}$	$.02128 < \varepsilon < .05935$[b]	1.366

[a] Yield stress: 0.822 GPa

[b] Upper limit of data

the Poisson effect. The dilatation Δ, is given by

$$\Delta = P/K \tag{19}$$

where P is the hydrostatic pressure, and K the bulk modulus. The hydrostatic pressure, given by $\sigma_{ii}/3$, is one-third the yield stress before the arrival of the slower, higher stress plastic waves. The computed dilatation is 0.20 percent strain, in excellent agreement with the experimental data as the demarcation between the two wave speeds for both regions of the rod, one-to-two and two-to-three rod diameters from the impact end. Using this value for the dilatation in Eq. (10) a dynamic yield stress of 0.949 GPa is computed, in close agreement with that computed by Eq. (11).

The progressive decrease of wave speeds above the bar wave velocity and simultaneous increase of those below that velocity is what must occur for the two-wave structure to collapse to the single bar wave velocity. An estimate can be made of the distance from the impact end where the two wave structure converges to the bar wave. Assume that the initial dilatational and shear velocities have accelerations such that each velocity will be equal to the bar wave velocity at the same point. For this to occur

$$(\overline{C}_1 - C_o)/(C_o - \overline{C}_2) = \text{constant} \tag{20}$$

everywhere along the rod, where $\overline{C}_1$ and $\overline{C}_2$ are the mode wave speeds of strains below and above the dilatation strain. Using the values of C_1 and C_2 to compute the ratio corresponding to the impact end, the constant is 0.351. The ratio corresponding to a position two and one-half rod diameters (midway between positions where arrival times were measured) is 0.358, thus establishing the validity of the assumption Eq. (20). Assuming constant accelerations, it is estimated that convergence occurs between six and seven diameter lengths from the impact end. That this type of collapsing two-wave structure could exist is shown by Bell[25] for annealed aluminum in the context of Truesdell's[26] general theory of waves in finite elastic strain.

The applicability of Bell's theory to the quasi-static deformation data, and the experimental evidence that wave speeds of post-yield strains were governed by a nearly parabolic stress-strain relation motivated an examination of the dynamic deformation data in the context of the theory. The exponent a in Eq. (18) was assumed equal to one-half, and the wave speed expression was linearized with respect to strain. Wave speed to the minus four power versus dynamic post-yield strain was found to be a linear relationship, as Figure 11 shows.

---

[25] *J. F. Bell, "Experiments on Large Amplitude Waves in Finite Elastic Strain," Proceedings, IUTAM Symposium on Second Order Effects in Elasticity, Plasticity, and Fluid Dynamics, Pergamon Press, 1964, pp 173-186.*

[26] *C. A. Truesdell, "General and Exact Theory of Waves in Finite Elastic Strain," Arch, Rational Mech. Anal., 8, No. 3, 1961, pp 263-352.*

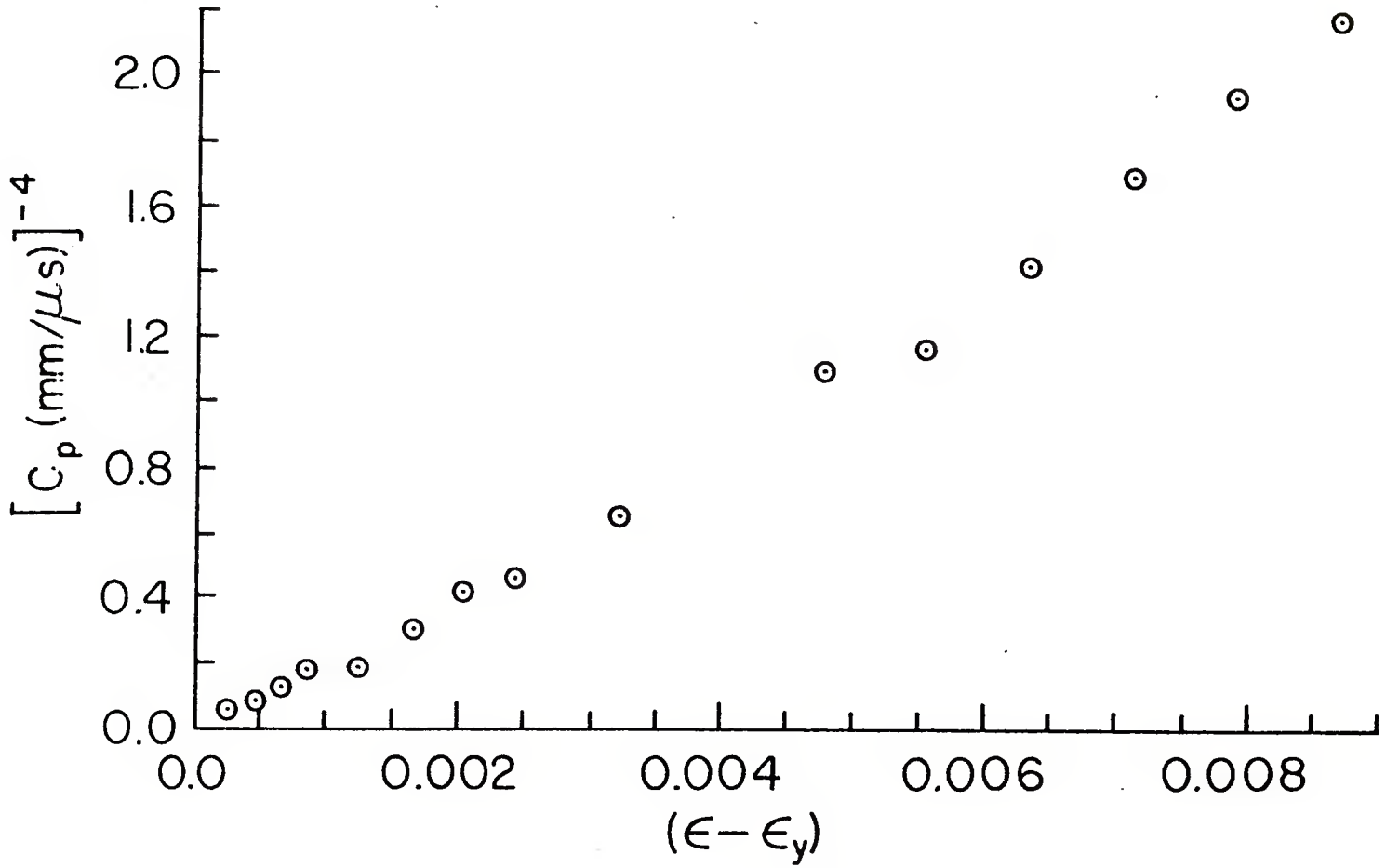

Figure 11. Linearized wave speed vs. dynamic post-yield strain data, assuming parabolic response function.

The value of the deformation modulus β, determined from the slope was 1.092 ± .030 GPa. This is within two percent of the quasi-static value for this strain region, and very close to theoretical prediction. It cannot be determined whether mode index changes occur at the transition strains for this material but Bell's investigations of many other materials show that mode index changes do not occur in dynamic loading, and that a single deformation modulus β, applies as long as stress and strain are monotonically increasing.[4] Wave speed versus strain is plotted in Figure 12, along with a graph of the theoretical curve

$$C_p = \sqrt{\beta/2\rho}\ (\varepsilon - \varepsilon_y)^{-1/4} \tag{21}$$

where β and ε_y are the experimentally determined values.

The fact that plastic wave speeds were found to propagate with constant velocity is a necessary, but not sufficient condition for the applicability of the strain-rate independent, one-dimensional, finite amplitude wave propagation theory. The first integral relationship [Eq. (14)] must be shown to apply. Particle velocity measurements at points along the rod were not made during deformation, so only the terminal condition of Eq. (14)

$$\dot{u}_{max} = \int^{\varepsilon_{max}} C(\varepsilon)\ d\varepsilon \tag{22}$$

could be checked with experiment. The maximum particle velocity can be partitioned into an elastic and plastic portion. The maximum elastic particle velocity $\dot{u}_y$, has been experimentally determined, and Eq. (21) predicts plastic wave speeds, thus:

$$\dot{u}_{max} = \dot{u}_y + (4/3)\sqrt{\beta/2\rho}\ \ (\varepsilon_{max} - \varepsilon_y)^{3/4} \tag{23}$$

The relatively slow velocity of the plastic wave fronts (compared to elastic waves), coupled with finite specimen lengths restricted the propagation distance of large strains because their amplitude was reduced by the reflected elastic precursor. However, low level plastic strains did propagate larger distances due to their higher velocity, and a plateau of maximum strain was observed on rods struck at low velocity. This can be seen in Figure 7, Test 20, where the maximum strain at 50 and 75 mm from the impact end is the same. This maximum strain is 0.515 percent and is predicted by Eq. (23) for the maximum particle velocity for this test. The maximum strain for the higher impact velocities did propagate unreduced at least the first rod diameter length from the impact end. It was assumed, as a first approximation, that the magnitude of the unloading strain had been equal to yield strain, and that the maximum strain was the sum of the yield strain and the permanent, or residual strain.

$$\varepsilon_{max} = \varepsilon_y + \varepsilon_\omega \tag{24}$$

That the residual strain measured at the first diameter position corresponded closely with the prediction of Eqs. (23) and (24) is shown in Figure 13 for rods with a maximum particle velocity of 0.040 mm/μs. The predicted residual strain is 1.678 percent, and the size of the symbol indicates the scatter of the individual measurements.

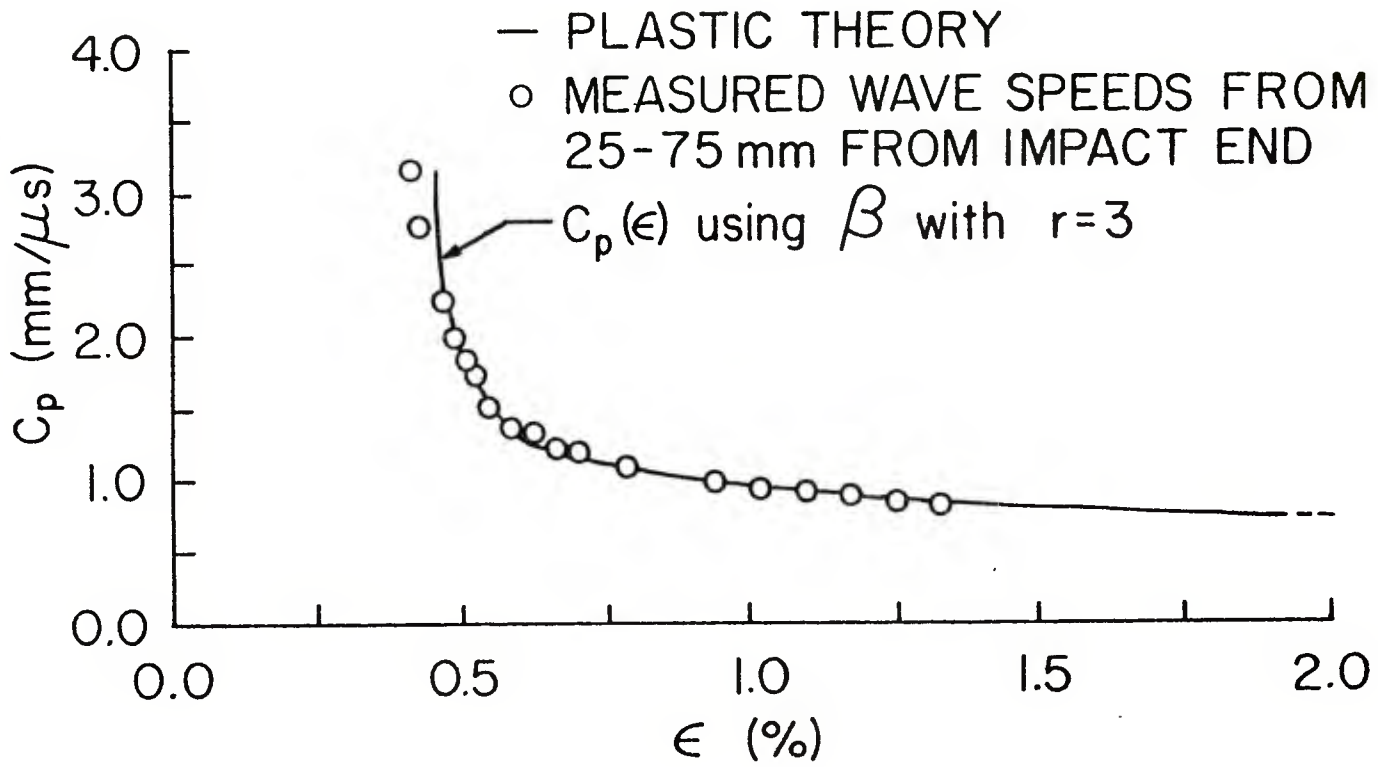

Figure 12. Wave speed vs. compressive strain compared with prediction of parabolic response function.

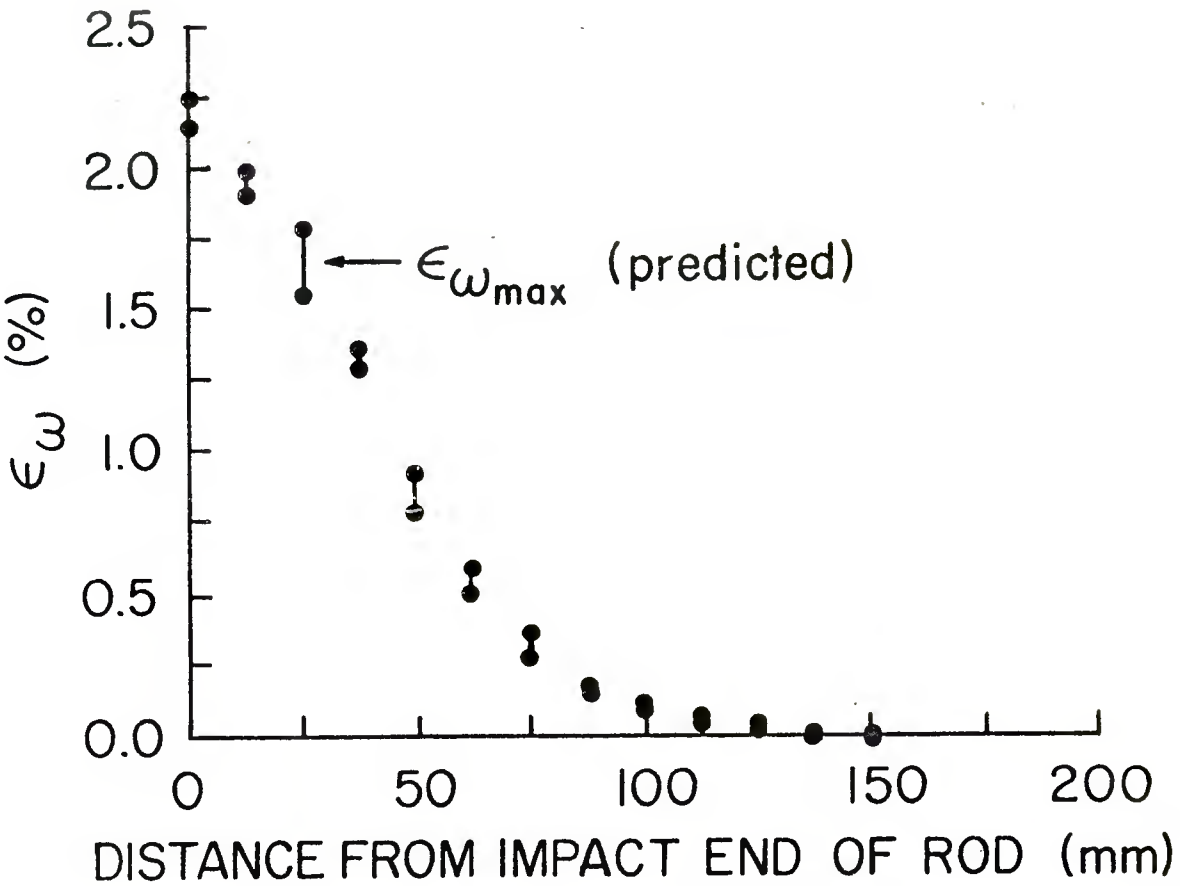

Figure 13. Residual strain vs. distance from impact end for rods struck at 80 m/s.

Strain maxima at one rod diameter length from the impact end were computed by Eq. (24), and are plotted in Figure 14 (circles) against the maximum particle velocity of the respective test. A graph of Eq. (23) with $\dot{u}_{max}$ as the independent variable (solid line) shows the correlation of the theory and experiment. The experimentally determined value of β (1.092 GPa) was used, and this single value of deformation modulus predicts the strain maxima even beyond the first transition strain of 1.960 percent. This is consistent with the observation that mode index changes do not occur in dynamic loading.[4]

The apparent departure of theory from experiment in predicting maximum strains for the higher impact velocities is due to the progressively decreasing validity of Eq. (24). Using momentum considerations, Lee[27] shows that the reflected elastic precursor is gradually absorbed as it encounters the propagating plastic wave front. This is mathematically described by

$$\delta\sigma = \sigma_y - (\rho C_o \dot{u}_b - \sigma_b)/2 \tag{25}$$

where the subscript b refers to values before the arrival of the unloading wave, and $\delta\sigma$ is the change in stress at the plastic wave front after passage of the unloading wave. Assuming linear elastic unloading, the unloading strain is given by

$$\varepsilon_{unl} = \delta\sigma/E \tag{26}$$

As particle velocity and stress increase, the magnitude of unloading strain approaches zero. If it is assumed that $\dot{u}_b$ is given by Eq. (23) and σ_b by Eq. (27) below for the same level of maximum strain, the strain maxima are given by the squares in Figure 14, which lie in closer agreement to theoretical prediction.

This correlation of theory and experiment in predicting maximum strains from wave speeds is deemed sufficient that the strain-rate independent, one-dimensional, finite amplitude wave propagation theory applies. Thus, dynamic stress is given by Eq. (15), which becomes

$$\sigma = \sigma_y + \beta(\varepsilon - \varepsilon_y)^{1/2} \tag{27}$$

when the wave speed expression [Eq. (21)] is the integrand, and the subscript y refers to dynamic yield values. Furthermore, the dynamic deformation modulus β is given by Eq. (6) for a mode index r = 3. The quasi-static and dynamic stress-strain curves are compared in Figure 15.

VI. SUMMARY AND CONCLUSIONS

Experimentally determined constitutive equations, which describe the quasi-static and dynamic response of thirty-eight millimeter thick RHA plate to uni-axial compression, are presented. The quasi-static post-yield stress-strain

---

[27] *E. H. Lee, "A Boundary Value Problem in the Theory of Plastic Wave Propagation," Quart. Appl. Math, 10, No. 4, 1953, pp 335-346.*

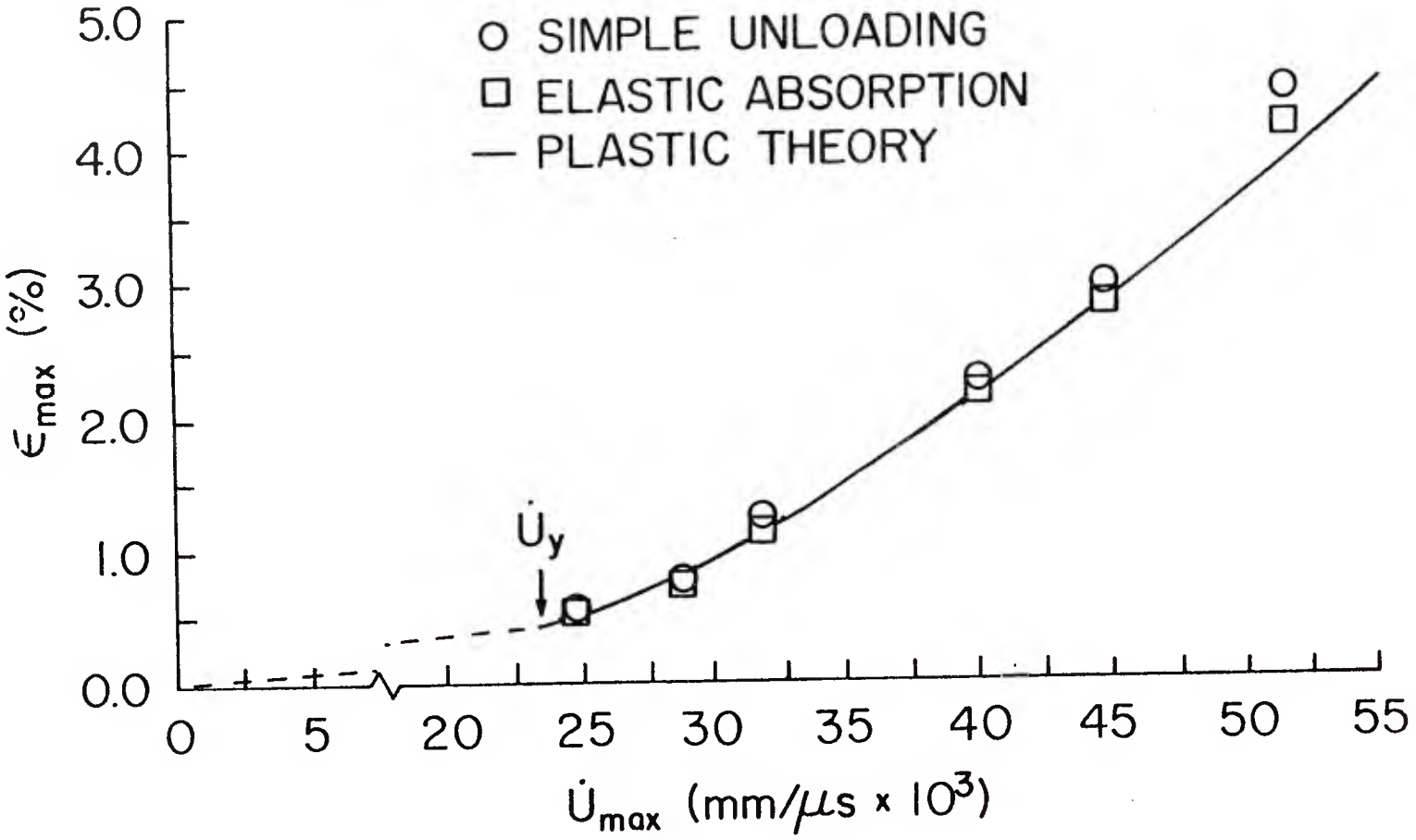

Figure 14. Maximum strain vs. maximum particle velocity compared with finite amplitude wave propagation theory using parabolic response function.

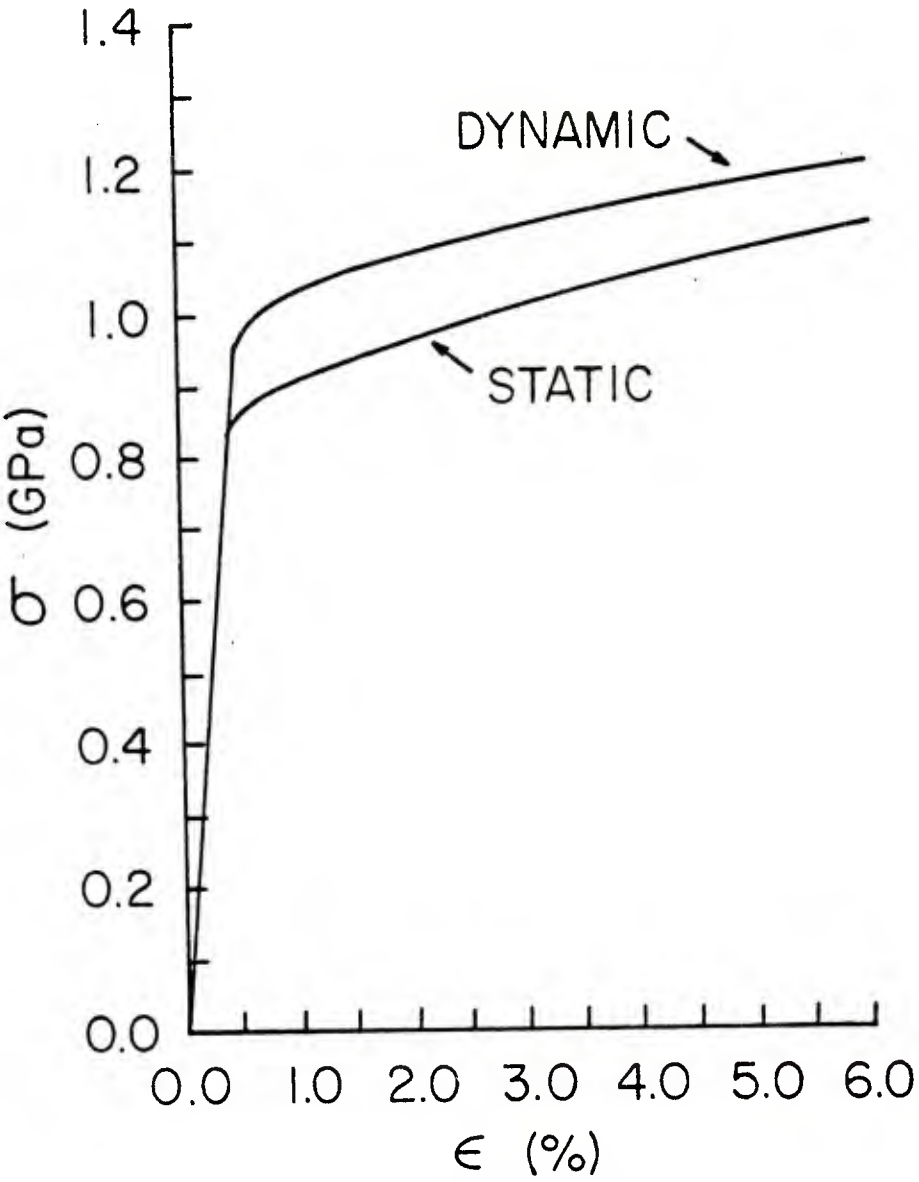

Figure 15. Comparison of static and dynamic stress-strain curves for 38 mm RHA.

response function, in nominal form, is parabolic with the origin at the yield point, corresponding to the intermediate region of Bell's general theory of parabolic plasticity. Two discrete deformation moduli characterize the response function. The change in modulus occurs at the first transition strain of the general theory, provided that the finite yield strain is accounted for. The moduli themselves compare favorably with those given by a single, quantized, temperature dependent relationship based on the value of the isotropic elastic shear modulus at absolute zero temperature.

The dynamic yield stress is higher than that measured in quasi-static loading, but is related to the latter in that the dynamic yield stress and the quasi-static stress at the first transition strain are equal. This suggests a material accommodation that is stress, not strain dependent. The dynamic stress-strain response function was deduced by using a one-dimensional, strain-rate independent, finite amplitude wave propagation theory, the applicability of which was shown experimentally. The dynamic response function also is parabolic, with its origin at the dynamic yield point. A single deformation modulus, nearly equal to the modulus of the initial portion of the quasi-static stress-strain curve, is applicable. This further relates the quasi-static and dynamic response functions. Wave propagation velocities and strain maxima near the impact end are well predicted by the wave propagation theory when the parabolic response function is inserted. However, strain arrival times and propagation distance of maximum strain are not, indicating that the maximum stress is not initiated as a step function at the impact face.

Elastic waves near the impact end do not propagate with a single velocity, but with a two-wave structure. Strains below the maximum expected dilatation propagate with the dilatational velocity, while elastic strains greater than the maximum dilatation propagate with the shear velocity. The trend of the data indicate that this two-wave structure degenerates to that of the bar wave at distances far from the impact end.

Although the strain range investigated is limited to six percent, deformation of RHA by uniaxial compression is explained by a general theory of plasticity for metal alloys.[4] The functional form of the response function is preserved over a strain rate range of seven orders of magnitude, and the increase in dynamic stress is attributable to the elastic, not plastic region. Additional experiments to extend and bridge the strain and strain-rate ranges investigated would provide the data needed to extend the applicability of the Bell theory to stresses and impact velocities of ballistic interest.

ACKNOWLEDGMENTS

The author is deeply grateful to Professor Emeritus James F. Bell of The Johns Hopkins University for his guidance in the application of his theory. The support and general guidance of Dr. Thomas W. Wright and Mr. Robert E. Franz are sincerely appreciated. The technical efforts of Messrs. John R. Stratton, Ralph F. Benck and Dominic A. DiBerardo, who assisted with the experiments and data reduction, are also thankfully acknowledged.

REFERENCES

1. R. F. Benck, "Quasi-Static Tensile Stress Strain Curves--II, Rolled Homogeneous Armor," BRL Memorandum Report No. 2703, Ballistic Research Laboratory, Aberdeen Proving Ground, Maryland, November 1976, AD #B016015L.

2. R. F. Benck, J. L. Robitaille, "Tensile Stress Strain Curves--III, Rolled Homogeneous Armor at a Strain Rate of 0.42 s^{-1}," BRL Memorandum Report No. 2760, Ballistic Research Laboratory, Aberdeen Proving Ground, Maryland, June 1977.

3. G. E. Hauver, "The Alpha Phase Hugoniot of Rolled Homogeneous Armor," BRL Memorandum Report No. 2651, Ballistic Research Laboratory, Aberdeen Proving Ground, Maryland, August 1976, AD #B012871L.

4. J. F. Bell, "A Physical Basis for Continuum Theories of Finite Strain Plasticity: Part I," Arch. Rational Mech. Anal., 70, 1979, pp 319-338, and "..... Part II," Arch. Rational Mech. Anal., 75, 1981, pp 104-126.

5. J. F. Bell, "On the Dynamic Elastic Limit," Exp. Mech., 22, No. 7, 1982, pp 270-276.

6. T. von Kármán, "On the Propagation of Plastic Deformation in Solids," National Defense Research Council Report A-29, OSRD 365, U.S.A., February 1942.

7. G. I. Taylor, "The Plastic Wave in a Wire Extended by an Impact Load," Civil Defense Research Committee Report R.C. 329, British Ministry of Home Security, 1942.

8. K. A. Rakhmatulin, "Propagation of a Wave of Unloading," Soviet J. Appl. Math., Mech., 9, 1945.

9. M. P. White, Le van Griffis, "The Permanent Strain in a Uniform Bar Due to Longitudinal Impact," J. Appl. Mech., 14, 1947, pp A-337 - A-342.

10. J. F. Bell, The Physics of Large Deformation of Crystalline Solids, Springer Tracts in Natural Philosophy, Vol. 14, Springer-Verlag, Heidelberg, Berlin, New York, 1968.

11. J. F. Bell, The Experimental Foundations of Solid Mechanics, Handbuch der Physik, Vol. VIa/1, Springer-Verlag, Heidelberg, Berlin, New York, 1973.

12. J. F. Bell, "Technological Perspectives from Two Decades of Fundamental Research in Dynamic Plasticity," BRL Contract Report No. 184, Ballistic Research Laboratory, Aberdeen Proving Ground, Maryland, October 1974, AD #A003175.

13. J. F. Bell, "Origins in Experiment of a New General Theory of Plasticity for Structural Metal Alloys," BRL Contract Report No. 311, Ballistic Research Laboratory, Aberdeen Proving Ground, Maryland, August 1976, AD #A029845.

14. J. F. Bell, "Generalized Large Deformation Behaviour for Face-Centered-Cubic Solids: Nickel, Aluminum, Gold, Silver, and Lead," Phil. Mag. 11, No. 114, 1965, pp 1135-1156.

15. J. E. Sears, "On the Longitudinal Impact of Metal Rods with Rounded Ends, Part II," Cambridge Phil. Soc., 21, 1912, pp 49-105.

16. H. Kolsky, Stress Waves in Solids, Dover Publications Inc., New York, 1963, pp 164-170.

17. Military Specification, Steel Armor: Plate Wrought Homogeneous; Combat Vehicle Type (1/4 to 6 inches, incl.), MIL SPEC MIL-S-12560B (ORD), 31 July 1962.

18. G. L. Kehl, Principles of Metallographic Laboratory Practice, McGraw-Hill Book Co., Inc., New York, 1949, pp 205-206, Table 28.

19. R. F. Benck, D. A. DiBerardo, R. E. Franz, "Quasi-Static Compression Tests - S7 Tool Steel," BRL Memorandum Report No. 0367, Ballistic Research Laboratory, Aberdeen Proving Ground, Maryland, October 1980.

20. J. F. Bell, "An Experimental Study of the Unloading Phenomenon in Constant Velocity Impact," J. Mech. Phys. Sol., 9, 1961, pp 1-15.

21. R. C. Weast, Ph.D, ed., Handbook of Chemistry and Physics, 56th Ed., The Chemical Rubber Co., Cleveland, 1975, p B-20.

22. S. Timoshenko and S. N. Goodier, Theory of Elasticity, McGraw-Hill Book Co., Inc., New York, 1951, p 444.

23. G. L. Filbey, "Intense Plastic Waves," Ph.D. Dissertation, The Johns Hopkins University, Baltimore, Maryland, 1961.

24. J. F. Bell, "The Initial Development of an Elastic Pulse Propagating in a Semi-Infinite Bar," BRL Technical Report No. 6, The Johns Hopkins University, Baltimore, Maryland, November 1960.

25. J. F. Bell, "Experiments on Large Amplitude Waves in Finite Elastic Strain," Proceedings, IUTAM Symposium on Second Order Effects in Elasticity, Plasticity, and Fluid Dynamics, Pergamon Press, 1964, pp 173-186.

26. C. A. Truesdell, "General and Exact Theory of Waves in Finite Elastic Strain," Arch. Rational Mech. Anal., 8, No. 3, 1961, pp 263-352.

27. E. H. Lee, "A Boundary Value Problem in the Theory of Plastic Wave Propagation," Quart. Appl. Math, 10, No. 4, 1953, pp 335-346.

LIST OF SYMBOLS

a	exponent, dimensionless
e	coefficient of restitution, dimensionless
r	deformation modulus mode index, dimensionless
t	time, μs
u	displacement, mm
B_o	deformation modulus constant, 0.0280
C	wave velocity, mm/μs
C_o	elastic bar wave velocity, mm/μs
C_1	elastic dilatational wave velocity, mm/μs
C_2	elastic shear wave velocity, mm/μs
D	specimen diameter, mm
E	Young's modulus, GPa
H	power function coefficient, GPa
K	bulk modulus, GPa
L	specimen length, mm
N	integer constant, dimensionless
P	hydrostatic pressure, GPa
R	strain gage resistance, ohms
R_o	initial resistance of unstrained strain gage, ohms
S	deformation modulus, GPa
T_a	ambient material temperature, degrees Kelvin
T_m	material melting temperature, degrees Kelvin
X	Lagrangian coordinate, mm
β	plastic deformation modulus, GPa
δ	change in quantity operator
ε	nominal engineering strain, mm/mm

ε_N	plastic transition strain, mm/mm
ε'_N	total transition strain, mm/mm
ε_{unl}	unloading strain, mm/mm
ε_ω	final, permanent strain, mm/mm
λ	Lamé's constant, GPa
μ	shear modulus, GPa
ν	Poisson's ratio, dimensionless
ρ	mass density, g/cm^3
σ	nominal engineering stress, GPa
Δ	dilatation, mm^3/mm^3

Subscripts

b	value of quantity before unloading
max	maximum value of quantity
p	quantity in plastic condition
y	value of quantity at yield

Superscripts

$\cdot$	first derivative with respect to time
$\overline{\quad}$	statistical mode value of quantity

DISTRIBUTION LIST

No. of Copies	Organization
12	Administrator Defense Technical Info Center ATTN: DTIC-DDA Cameron Station Alexandria, VA 22314
1	Deputy Assistant Secretary of the Army (R&D) Department of the Army Washington, DC 20310
1	HQDA (DAMA-ARP-P, D. Watson) Washington, DC 20310
1	HQDA (DAMA-MS) Washington, DC 20310
1	Commander US Army Materiel Development and Readiness Command ATTN: DRCDMD-ST 5001 Eisenhower Avenue Alexandria, VA 22333
1	Commander US Army Armament Research and Development Command ATTN: DRDAR-TDC (Dr. D. Gyorog) Dover, NJ 07801
4	Commander US Army Armament Research and Development Command ATTN: DRDAR-TSS DRDAR-SC, Dr. E. Bloore DRDAR-LC, Dr. J. Frasier Dover, NJ 07801
1	Director US Army Armament Research and Development Command Benet Weapons Laboratory ATTN: DRDAR-LCB-TL Watervliet, NY 12189
1	Commander US Army Armament Materiel Readiness Command ATTN: DRSAR-LEP-L Rock Island, IL 61299
1	Commander US Army Aviation Research and Development Command ATTN: DRDAV-E 4300 Goodfellow Blvd St. Louis, MO 63120
1	Director US Army Air Mobility Research and Development Laboratory Ames Research Center Moffett Field, CA 94035
1	Director US Army Research and Technology Laboratories Applied Technology Laboratory Fort Eustis, VA 23604
1	Commander US Army Communications Research and Development Command ATTN: DRDCO-PPA-SA Fort Monmouth, NJ 07703
1	Commander US Army Electronics Research and Development Command Technical Support Activity ATTN: DELSD-L Fort Monmouth, NJ 07703
1	Commander US Army Harry Diamond Lab. ATTN: DELHD-TA-L 2800 Powder Mill Road Adelphi, MD 20783
1	Director US Army Advanced BMD Technology Center ATTN: CRDABH-5, W. Loomis P. O. Box 1500 Huntsville, AL 35804
1	Commander US Army Ballistic Missile Defense Systems Command P. O. Box 1500 Huntsville, AL 35804

DISTRIBUTION LIST

No. of Copies	Organization
1	Director US Army Ballistic Missile Defense Program Office 5001 Eisenhower Ave. Alexandria, VA 22333
1	Commander US Army Missile Command ATTN: DRSMI-R Redstone Arsenal, AL 35898
1	Commander US Army Missile Command ATTN: DRSMI-YDL Redstone Arsenal, AL 35898
2	Commander US Army Mobility Equipment Research and Development Command ATTN: DRDME-WC DRSME-RZT Fort Belvoir, VA 22060
1	Commander US Army Natick Research and Development Center ATTN: DRDNA-DT, Dr. D. Sieling Natick, MA 01762
1	Commander US Army Tank Automotive Research and Development Command ATTN: DRDTA-UL Warren, MI 48090
3	Commander US Army Materials and Mechanics Research Center ATTN: DRXMR-T, J. Mescall DRXMR-T, R. Shea DRXMR-H, S. C. Chou Watertown, MA 02172
3	Commander US Army Research Office ATTN: Dr. G. Mayer Dr. F. Schmiedeshoff Dr. E. Saibel P. O. Box 12211 Research Triangle Park NC 27709
1	Director US Army TRADOC Systems Analysis Activity ATTN: ATAA-SL, Tech Lib White Sands Missile Range NM 88002
1	Commander US Army Command and General Staff College ATTN: Archives Fort Leavenworth, KS 66027
1	Commander US Army War College ATTN: Lib Carlisle Barracks, PA 17013
1	Commander US Military Academy ATTN: Library West Point, NY 10996
1	Chief of Naval Research Department of the Navy ATTN: Code 402 Washington, DC 20360
1	Commander US Naval Weapons Center ATTN: Code 3835, Mr. Backman China Lake, CA 93555
1	Commander US Naval Surface Weapons Center ATTN: Code Gr-9, Dr. W. Soper Dahlgren, VA 22448

DISTRIBUTION LIST

No. of Copies	Organization
1	Commander US Naval Surface Weapons Center ATTN: Code R-32, Dr. S. Fishman Silver Spring, MD 20910
4	Commander US Naval Research Laboratory ATTN: Code 5270, F. MacDonald Code 2020, Tech Lib Code 7786, J. Baker C. Sanday Washington, DC 20375
4	AFATL ATTN: DLDG DLDL, Maj. J. D. Morgan DLYW J. Smith Eglin AFB, FL 32542
1	AFFDL/FB (Dr. J. Halpin) Wright-Patterson AFB, OH 45433
3	Honeywell, Inc. Government and Aerospace Products Division ATTN: Dr. G. Johnson Mr. J. Blackburn Mr. R. Simpson 600 Second Street, NE Hopkins, MN 55343
2	Director Lawrence Livermore Laboratory ATTN: Dr. M. Wilkins Dr. M. von Thiel P. O. Box 808 Livermore, CA 94550
3	Los Alamos Scientific Laboratory ATTN: Tech Lib Dr. J. Taylor Dr. R. Karpp P. O. Box 808 Livermore, CA 94550
4	Sandia National Laboratories ATTN: Dr. L. Davison Dr. P. Chen Dr. L. Bertholf Dr. W. Herrmann Albuquerque, NM 87115
4	SRI International ATTN: D. Curran L. Seaman Y. Gupta G. R. Abrahamson 333 Ravenswood Avenue Menlo Park, CA 94025
5	Brown University Division of Engineering ATTN: Prof. R. Clifton Prof. H. Kolsky Prof. A. Pipkin Prof. P. Symunds Prof. J. Martin Providence, RI 02912
3	California Institute of Technology Division of Engineering and Applied Science ATTN: Dr. J. Miklowitz Dr. E. Sternberg Dr. J. Knowles Pasadena, CA 91102
1	Drexel Institute of Technology Wave Propagation Research Center ATTN: Prof. P. C. Chou 32nd and Chestnut Streets Philadelphia, PA 19104
1	Harvard University Division of Engineering and Applied Physics ATTN: Dr. G. Carrier Cambridge, MA 02139
1	Iowa State University Department of Engineering Science and Mechanics ATTN: Dr. C. P. Burger Ames, IA 50010

DISTRIBUTION LIST

No. of Copies	Organization
2	Iowa State University Engineering Research Lab. ATTN: Dr. G. Nariboli Dr. A. Sedov Ames, IA 50010
1	Louisiana State University Department of Mechanical Engineering ATTN: Prof. W. Sharpe Baton Rouge, LA 70803
1	Massachusetts Institute of Technology ATTN: Dr. R. Probstein 77 Massachusetts Avenue Cambridge, MA 02139
2	Southwest Research Institute Department of Mechanical Sciences ATTN: Dr. U. Lindholm Dr. W. Baker 8500 Culebra Road San Antonio, TX 78228
4	Falcon Research & Dev Corp ATTN: Prof. J. Bell Prof. R. Green Prof. R. Pond, Sr. Prof. C. Truesdell 696 Fairmont Ave. Towson, MD 21204
1	University of California at Los Angeles Department of Mechanics ATTN: W. Goldsmith Los Angeles, CA 90024
2	University of Dayton University of Dayton Rsch Inst ATTN: A. M. Rajendran S. J. Bless Dayton, OH 45406
2	University of Delaware Department of Mechanical Engineering ATTN: Prof. J. Vinson Dr. M. Taya Newark, DE 19711
2	Washington State University Department of Physics ATTN: Prof. G.E. Duvall Prof. R. Fowles Pullman, WA 99164
2	University of Illinois at Chicago Circle College of Engineering Dept. of Materials Engineering ATTN: Prof. A. Schultz Dr. T.C.T. Ting P. O. Box 4348 Chicago, IL 60680
2	University of Minnesota Department of Engineering Mechanics ATTN: Dr. R. Fosdick Dr. J. Ericksen Minneapolis, MN 55455

Aberdeen Proving Ground

Dir, USAMSAA
ATTN: DRXSY-D
DRXSY-MP, H. Cohen
Cdr, USATECOM
ATTN: DRSTE-TO-F
Dir, USACSL, Bldg. E-3516, EA
ATTN: DRDAR-CLB-PA

USER EVALUATION OF REPORT

Please take a few minutes to answer the questions below; tear out this sheet, fold as indicated, staple or tape closed, and place in the mail. Your comments will provide us with information for improving future reports.

1. BRL Report Number _____

2. Does this report satisfy a need? (Comment on purpose, related project, or other area of interest for which report will be used.)

_____

_____

_____

3. How, specifically, is the report being used? (Information source, design data or procedure, management procedure, source of ideas, etc.) _____

_____

_____

4. Has the information in this report led to any quantitative savings as far as man-hours/contract dollars saved, operating costs avoided, efficiencies achieved, etc.? If so, please elaborate.

_____

_____

5. General Comments (Indicate what you think should be changed to make this report and future reports of this type more responsive to your needs, more usable, improve readability, etc.) _____

_____

_____

_____

6. If you would like to be contacted by the personnel who prepared this report to raise specific questions or discuss the topic, please fill in the following information.

Name: _____

Telephone Number: _____

Organization Address: _____

_____

_____